In-situ observations of microstructural changes during hot deformation and modelling of grain growth at high temperatures

By

Yasuhiro YOGO

TOYOTA CENTRAL R&D LABS., INC.

A dissertation submitted for

the degree of Doctor of Engineering

at the Nagoya University

2011

Abstract:

In order to develop a theoretically based prediction method for grain size change during recrystallization, detailed investigation according to observation results is first step. In this thesis, a new *in-situ* observation method was first developed. This method enables us to directly observe microstructural changes at high temperatures. An experimental device to conduct *in-situ* observation is composed of a hot deformation type thermo-mechanical simulator and a confocal scanning laser microscope. By the *in-situ* observation method, observations for some kinds of microstructural changes were conducted: grain growth, strain induced grain boundary migration under small strains, dynamic recrystallization, inverse phase transformation and phase transformation. Through those observations at high temperatures, possibility and usefulness of the *in-situ* observation method was confirmed. In particular, it was shown that the *in-situ* observation method could be applied to observations during hot deformation. In the following, theoretically based prediction method for grain growth at high temperatures is proposed. This method is based on the solute drag theory. This is placed on a foundation of the theoretically based prediction method for grain size change during recrystallization.

Contents:

Chapter 1:

Introduction

1. 1. Overview

In order to strengthen metallic materials especially for steels, there are four methods to change and improve microstructural properties; solid solution, precipitation, work hardening and grain size refinement. Through the long history of steels, researchers have developed various kinds of methodology to apply such strengthening mechanisms to steels in order to bring out their potentials. Adding alloying elements is also a method to produce industrial high strength parts. Appling heat treatment after shaping parts is another method for that purpose as well. However, because of manufacturing costs, less alloying and manufacturing processes are desirable. When considering recycling, decreasing both contents and kinds of alloying elements are preferable. Due to such recent manufacturing trends, the strengthening mechanism of grain size refinement is a hot research focus. The effectiveness of grain refinement to strengthen steels is explained by a famous empirical and experimental law, which relates grain size and mechanical property, called the Hall - Petch law. [1.1], [1.2] According to the law, strength is proportional to grain size power (-1/2) ($\sigma_y = A\sqrt{d}$. Here σ_y is yield stress, d is mean grain size and A is a material constant). That is, decreasing grain size increases strength. In the case of steels, recrystallization and inhibiting grain growth are the most effective ways to achieve grain refinement.

Refining grain size by recrystallization was first actively applied to producing line pipe in 1960s. [1.3] Next, several research groups have associated the relationship between recrystallized grain size and deformation conditions, and made experimentally based equations to predict grain size, especially for low carbon steels and Nb alloyed steels. [1.4], [1.5] Such research results gave significant impact on other research groups and helped to improve controlled-rolling-technology. On the other hand, it is pointed out that applicable range of such equations is limited. The calculated values based on empirical equations are reliable in the range of the experiments conducted. However, extrapolated range of the experiment, for example temperature range and alloying contents and kinds range, reliability of calculated values are not always high. As shown in the references [1.4], [1.5], making such equations requires many experiments, and the number of experiments affects accuracy of the equations. Therefore, it is difficult to obtain new equations for extending applicable range of the equations. There is another difficulty. That is the equations for predicting recrystallized grain size are based not on theoretical descriptions but on statistical works of experimental results. That makes extending their applicable range for alloying elements more difficult. Meanwhile, prediction methods for phase transformation from austenite to ferrite and pearlite, and precipitation is constructed by theoretical and mathematical consideration. [1.6] ,[1.7], [1.8] Those are modeled by "nucleation and growth". These modeling methods can cover a wide range of alloying elements by coupling with thermodynamics calculations. [1.9], [1.10], [1.11] Compared with the prediction method of phase transformation, the prediction method of recrystallization has not been improved yet in terms of capability to cover various kinds of alloying elements.

There are two reasons that the prediction method of recrystallization for steels is undergoing development. The first reason is that recrystallization is a very fast phenomenon. Therefore, accurate experiments to observe and measure grain size change are difficult. The second reason is that recrystallization of steels occurs at high temperature. Therefore it is not possible to observe the changing of grains directly. With a conventional experimental method to understand recrystallization of steels, these experimental procedures are usually applied; a specimen is first heated up to the predefined temperature (it is mostly over Ac3 temperature for carbon steels), next it is deformed, and then quenched in water or He gas. The quenched specimen is cut and polished to a mirrored surface and then etched by Picral or Nital or some other kinds of etching agents to reveal grain boundary. Finally, microstructures are observed at room temperature. [1.12] Quenching must be done to stop microstructural changes of recrystallized grains immediately. This is one of the most crucial points of the procedure, as microstructural changes during and after recrystallization are very quick, so special experimental devices are required to allow researchers to quench specimens in required time accurately. As it is known, those experimental procedures have improved understanding of recrystallization for steels, and those results have been well summarized. [1.13], [1.14], [1.15] However, with those experimental procedures, researchers can only observe microstructure after the specimen has been quenched. It is obvious that researchers have difficulties distinguishing recrystallized grains from other grains, they cannot know the history of grains focused on, and only can infer their history. It is well known that recrystallized grains have less dislocation than un-recrystallized grains. Therefore, crystallographic analysis to measure dislocations or strains in grains can help

to distinguish recrystallized grains. However, in the case of carbon steels, microstructure is always transformed from austenite to other phases during cooling. As a result of that, crystallographic analysis cannot be applied to analyze recrystallized grains. If we could observe microstructural changes at high temperatures at which recrystallization can occur, almost all difficulties mentioned above would be solved. *In-situ* observation (direct observation) gives us enough information to understand recrystallization, to distinguish recrystallized grains from others, and to know grain size evolution which helps us in making equations for predicting grain size during recrystallization.

1. 2. Purpose and strategy

The purpose of this work is to develop an *in-situ* observation method for microstructural changes during hot deformation. The target materials are carbon steels. The development is conducted in four steps. In the first step of the development in chapter 2, *in-situ* observation method is developed and observations are conducted in stable conditions (without deformation) at high temperatures. In the second step in chapter 3, observations of microstructural changes during small deformation at high temperatures are conducted. In these observations, strain induced boundary migrations (SIBM) are observed. In the third step in chapter 4, progress of recrystallization by hot deformation is observed. In the fourth step, inverse phase transformation and phase transformation are observed in chapter 5. A modeling method for grain growth at high temperatures is proposed as well in chapter 6. This modeling is based on theoretical descriptions by the solute drag theory and coupled with thermodynamics calculations.

Therefore, it would be applicable to a wide range of carbon steels, especially for microalloyed steels. That method would be the first development of the prediction method as a foundation of a new theoretically based prediction method for recrystallization.

Reference

[1.1] E.O.Hall, Proc. Phys. Soc., Ser. B, 64 (1951), pp. 747-753

[1.2] N.J.Petch, J. Iron and Steel Institute, (1953), pp. 25-28

[1.3] Isao Kozasu, Seigyo-atsuen seigyo-reikyaku, (1997), ed. The Iron and Steel Institute of Japan, Tijin-syokan, (in Japanese)

[1.4] C. M. Sellars and J.A. Whiteman: Met. Sci., 13 (1979), 187-194.

[1.5] T. Senuma, H. Yada, Y. Matsumura and T.Futamura: Tetsu to Hagane, 15 (1984), 2112-2119. (in Japanese)

[1.6] M. Suehiro, T. Senuma, H. Yada, Y. Matsumura and T. Ariyoshi: Tetsu to Hagane, 73 (1987) 1026-33. (in Japanese)

[1.7] M. Umemoto, A. Hiramatsu, A. Moriya, T. Watanabe, S. Nanba, N. Nakajima, G. Anan and Y. Higo: ISIJ Int., 32 (1992), 306-315.

[1.8] W. F. Lange, M. Enomoto and H. I. Aaronson: Metall. Trans. 19A (1988) 427-440.

[1.9] J. Ågren: Current Opinion in Solid State & Materials Science, 1996, vol. 1, pp. 355-60.

[1.10] B. Sundman: Scand. J. Metall., 1991, vol. 20, pp. 79-85.

[1.11] B. Jansson, B. Jönsson, Bo. Sundman, and J. Ågren: Thermochimica Acta, 1993, vol. 214, pp. 93-96.

[1.12] Hiroshi Yada, Nobuhiko Matuzu, Yoshikazu Matsumura and Jiro Tominaga, Tetsu-to-Hagane, 15 (1984), p.338-345. (in Japanese)

[1.13] Proceeding of THERMEC-88, ed. I Tamura, (1988).

[1.14] 131,132th Nishiyama-Kinen-kouza, (1989), the Iron and Steel Institute of Japan.

[1.15] F. J. Humphreys, M. Hatherly. Recrystallization and Related Annealing Phenomena Second edition, Elsevier, Oxford, (2004).

Chapter 2:

Development of in-situ observation method for microstructural changes at high temperatures

2. 1. Background

In conventional studies, researchers have measured the relationships between grain size and holding time at various high temperatures to comprehend the microstructural changes, and these results have been used to predict the grain size during and after hot rolling and hot forging. [2.1], [2.2], [2.3], [2.4], [2.5]

In the case of using the conventional observation method for an austenite structure, a specimen is first heated to a predefined temperature and maintained at that temperature for a predefined time. The specimen is then cooled to room temperature by water or He gas. This preprocess is shown in **Figure 2. 1**. Next, the specimen is cut, and the cut plane is polished to a mirrored surface and etched by Picric acid or another etching agent. Finally, the grain size is quantified. With the conventional observational method, many specimens are required to measure the relationships between grain size and heating condition. For example, in the case of quantifying grain size at 30-second intervals while maintaining the temperature at 1,473 K (1200°C) for 10 minutes, 20 specimens were required. Thus, it is easy to imagine that the preparation procedure needed at each quantification is time consuming.

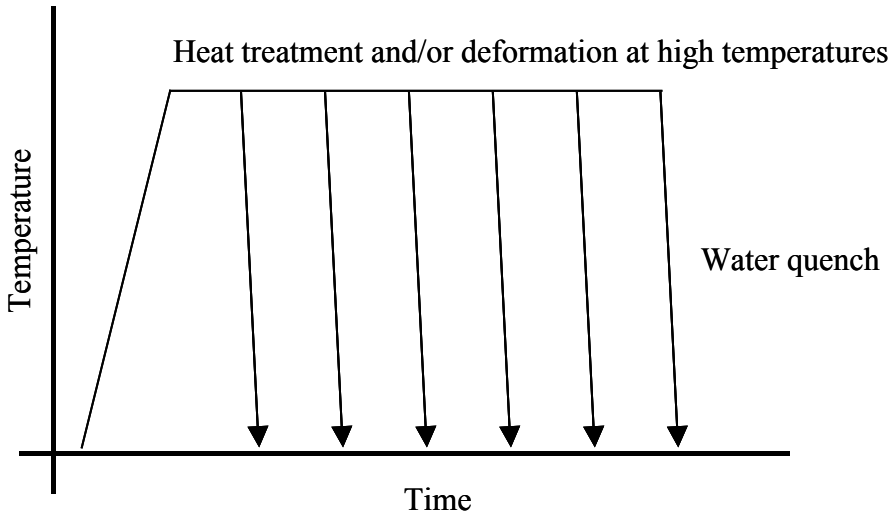

Figure 2. 1. Thermal and mechanical history for a preprocess of the conventional process to investigate microstructural changes at high temperatures.

2. 2. Purpose of this study

With respect to the conventional observation method, there are three problems. The first is that the initial structure of each specimen differs from each other during the entire process of measuring the relationship between grain sizes and heating condition. Therefore, the quantified data contain errors due to differences in the initial structure. The second problem is that the quantified data must be an average one taken from many grains in an observed area because of the difference in the initial structure. Therefore, it is not possible to quantify the size change for specified grains. The third problem is that dynamic changes of microstructure at high temperatures cannot be observed because observation is carried out at room temperature. Therefore, dynamic changes of microstructure are inferred by the observation results at room temperature.

If an observation being capable of quantifying the microstructural changes that occur at high temperatures is carried out using a single specimen for the entire process, it becomes possible to overcome each problem that hinders proper data collection. In this chapter, a new method for observing austenite structure at high temperatures is developed based on the above-mentioned concept.

2. 3. Experimental devices for observing microstructural changes

As mentioned up to here in this chapter, it is difficult to observe microstructural changes at high temperatures. However in the case of steels, the

temperature range over 1273 K (1000^{o}C) is very important to control microstructural chages, because high temperature phenomena, such as recrystallization and grain growth, occur. In this section, a couple of observation methods or devices, which enables us to observe microstructures, are reviewed. In the following, the most suitable method or device for observations at high temperatures is discussed in section 2.3.5.

2. 3. 1. X-ray diffraction measurement

X-ray diffraction measurement is one of the measurement methods of X-ray crystallography. X-ray crystallography is applied to determine the arrangement of atoms within a crystal. An X-ray beam strikes a crystal and diffracts into many specific directions. From the angles and intensities of these diffracted beams, a crystallographer can produce a three-dimensional picture of the density of electrons within the crystal. From this electron density, the mean positions of the atoms in the crystal, as well as their chemical bonds, their disorder and various other information, can be determined.

In an X-ray diffraction measurement, a crystal is mounted on a goniometer and gradually rotated while being bombarded with X-rays, producing a diffraction pattern of regularly spaced spots known as reflections. The two-dimensional images taken at different rotations are converted into a three-dimensional model of the density of electrons within the crystal using the mathematical method of Fourier transforms, combined with chemical data known for the sample. X-ray diffraction techniques are based on the elastic scattering of X-rays from structures that have long range order. The most comprehensive description of scattering from crystals has been summarized. [2.6]

Some synchrotron radiation facilities have been constructed in last two decades: SPring-8 (1997) in Japan, APS (1996) in USA and ESRF (1994) in France. The X-rays given by such synchrotron radiation facilities are high-energy X-rays. Therefore, these take shorter time to measure and can make a smaller focus than standard X-ray diffraction devices. Using high-energy X-rays given by such synchrotron radiation facilities, *in-situ* observations can be conducted. By installing a device to heat specimens on a beam line of X-ray, phase changes at high temperatures can be detected. Observations of solidifications of martensitic steel is reported.[2.7] Phase transformation and dynamic recrystallization of titanium aluminide alloy are observed by evaluating the occupancy and spottiness of the diffraction rings. [2.8]

2. 3. 2. Electron Back Scattering Pattern (EBSP) [2.9]

Electron Back Scattering Pattern (EBSP) is also known as Electron backscattered diffraction (EBSD) or backscattered Kikuchi diffraction. EBSP is a microstructural-crystallographic technique used to examine the crystallographic orientation of many materials for texture or orientation of polycrystalline materials. EBSP can be applied to crystal orientation mapping, phase identification, grain boundary studies, regional heterogeneity investigations, microstrain mapping and so on. These types of studies have been traditionally carried out using x-ray diffraction (XRD) or electron diffraction in a TEM.

Experimentally EBSD is conducted by using a Scanning Electron Microscope

(SEM) equipped with a backscatter diffraction camera. The diffraction camera consists of a screen, which is inserted into the specimen chamber of the SEM, and a CCD camera on the end of a light pipe to register the image on the screen. A flattened and polished crystalline specimen is placed into the normal position in the specimen chamber, but is sharply tilted (~70° from horizontal) towards the diffraction camera. When the electrons impinge on the specimen they interact with the atomic lattice planes of the crystalline structures, many of these interactions satisfy Bragg conditions and undergo backscatter diffraction. Due to the angle of the specimen, these diffracted electrons can escape the material and are directed towards and collide with the screen of the diffraction camera causing it to fluoresce, this fluorescent light is then detected by a low light CCD. The diffracted electrons produce a diffraction pattern, sometimes called an Electron Backscatter Pattern.

If the device to heat a specimen up can be installed into a chamber of SEM, observations for specimens at high temperatures can be conducted. However, there are three obstacles which must be overcome to apply EBSP to observations for high temperature phenomena. The first one is heat resistance. The second one is measurement noise. When a specimen is heated up to high temperatures, it emits high intensity light. That light disturbs a detector. Observation temperature is limited by the heat resistance of the screen to detect diffraction patterns. As far as I know, the maximum temperature conducted up to now is 1073 K (800°C). It is not high enough to observe dynamic recrystallization of steels. Third obstacle is measurement rate. It is very time consuming to conduct EBSP analysis. For example, it takes about 3 minutes to conduct EBSP analysis for 150 * 300 micro-meters (measurement interval: 2.5 μm,

total measurement points: 8410). [2.10]

2. 3. 3. Optical microscope

The optical microscope uses visible light and a system of lenses to magnify images of small samples. There are two basic configurations of the optical microscope; a single lens type and a compound lenses type. The vast majority of modern research microscopes are compound microscopes. Many sources of light can be used. Normally a halogen lamp is applied to most microscopes.

2. 3. 4. Laser microscope [2.11]

The laser microscope is one kinds of optical microscope. It applies laser to a source of light, and scans the surface of a specimen with focused laser light. Almost all laser microscopes are constructed using the optical system. Confocal laser scanning microscopy (CLSM or LSCM) is a technique for obtaining high-resolution optical images with depth selectivity. The key feature of confocal microscopy is its ability to acquire in-focus images from selected depths, a process known as optical sectioning. Images are acquired point-by-point and reconstructed with a computer, allowing three-dimensional reconstructions of topologically-complex objects.

In a confocal laser scanning microscope, a laser beam passes through a light source aperture and then is focused by an objective lens into a small (ideally diffraction

limited) focal volume within or on the surface of a specimen. The beam is scanned across the sample in the horizontal plane by using one or more (servo controlled) oscillating mirrors.

The detector aperture obstructs the light that is not coming from the focal point, as shown by the dotted gray line in the image. The out-of-focus light is suppressed: most of the returning light is blocked by the pinhole, which results in sharper images than those from conventional fluorescence microscopy techniques and permits one to obtain images of planes at various depths within the sample.

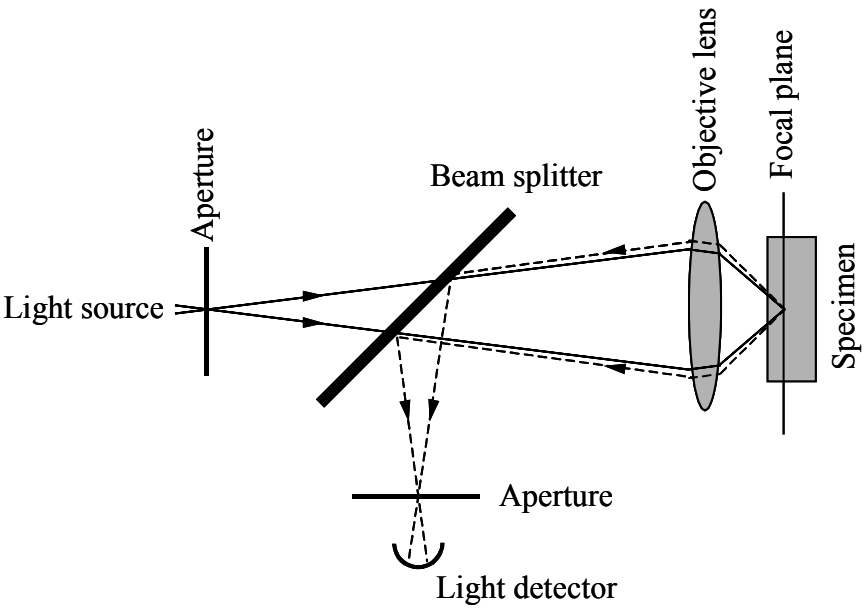

Figure 2. 2. schematic diagram of laser microscopy.

2. 3. 5. Summary of observation devices suitable for high temperature observations

In order to observe microstructural changes at high temperatures, some characteristics are required: (1) shorter analyzing or focusing time than microstructural changes, (2) high thermal resistance, (3) robustness for noise, and (4) easiness for observations.

X-ray diffraction measurement takes several seconds to analyze each point using a standard XRD device. If the large synchrotron radiation facilities can be applied, it would be possible to analyze fast microstructural changes, such as recrystallization, in real time. However, using a large synchrotron facility is not easy. Thermal resistance of EBSP is not high enough to conduct observation over 1273 K (1000 ^{0} C) for recrystallization and grain growth. The light source of an optical microscope is not strong. Therefore, because of strong light emitted from a specimen surface at high temperatures, a clear image cannot be obtained by optical microscope. On the other hand, with a laser microscope, scanning time is short enough to observe fast microstructural changes, and the light source is stronger than emitted light from the specimen. If a configuration, which can prevent thermal radiation heat from a specimen to the lens of the laser microscope, can be constructed, the laser microscope would have the possibility to conduct observations for specimen at high temperatures. As a result, applying laser microscope to observations at high temperatures would be the high potential choice available to date.

2. 4. Proposed observation device

In order to observe austenite structures at high temperature, the observation method must overcome two difficulties: (1) how does the method reveal the grain boundary and (2) how does the method observe austenite structure at high temperatures.

For revealing grain boundary, the thermal etching method [2.12], [2.13] is applied to the new observation device. The thermal etching method can reveal austenite grain boundary at high temperatures, because atoms diffuse and vaporize into the atmosphere from the grain boundary at a much higher rate than from the rest of the specimen, which leaves grooves that can be measured to determine the boundary. The quantified results using the thermal etching method are the same as the quantified results using the conventional observation method, which proves that the thermal etching method is reliable. [2.14] The schematic image of mechanism of the thermal etching method is shown in Figure 2. 3.

The new observation device is composed of two units, a hot deformation type thermo-mechanical simulator, THERMECMASTOR-Z, which can control the heating condition, atmosphere, hot deforming condition, and cooling condition, and a confocal scanning violet laser microscope, VL2000DX. A violet laser-diode is applied to the laser microscope. A laser microscope is generally more functional than an optical microscope in terms of images of resolution and the depth of focus. Figure 2. 4 shows the schematic layout of the new observation device. A specimen is heated by Joule heating and the temperature is controlled with a type R thermocouple. If a specimen is

firmly fixed at both the upper and lower ends, it buckles due to thermal expansion during heating. To avoid buckling, a specimen is hung from the upper end only, while at the lower end the clearance is set to allow for thermal expansion. The distance from the surface of a specimen to the observation window is very close, so it is exposed to a large amount of radiation heat. Therefore, to protect the observation window from extreme heat, the window is cooled by a water-filled tube.

In order to obtain clearer images, the surface of each specimen is polished to a mirrored surface, i.e., Rz = 0.1 μm. Figure 2. 5 shows the shape of the specimen. Figure 2. 6 shows comparison of observed images depending of surface roughness. When polishing on the specimen surface is not sufficient, scratches remain and deteriorate the observed images.

While observing an austenite structure, the atmosphere in the chamber must be maintained at an optimal condition in order to prevent oxidation of the specimen and the obstruction of the observation window. It is easy to imagine that oxygen in the chamber causes a specimen to oxidize, thereby making it impossible to determine grain boundaries. At high temperatures, atoms are diffused and vaporized into the atmosphere in the chamber from the surface of the specimen. The diffusion and vaporization of atoms reveals grain boundaries, but these atoms also obstruct the view through the observation window. Therefore, the atmosphere in the chamber is prepared by the following procedure. The atmosphere in the chamber is first vacuumed to less than 3×10^{-3} Pa and then filled with Ar gas. During the observation Ar gas is blown against the observation window, both to prevent the deposition of diffused and vaporized atoms and

to cool the window. This observation device is equipped with a hydraulic ram press and gas/water nozzle in a champer. Therefore, it is also possible to observe microstructural changes during hot deformation and cooling.

These configurations of the new observation device and the atmosphere treatment make it possible to observe the revealed grain boundaries at high temperature.

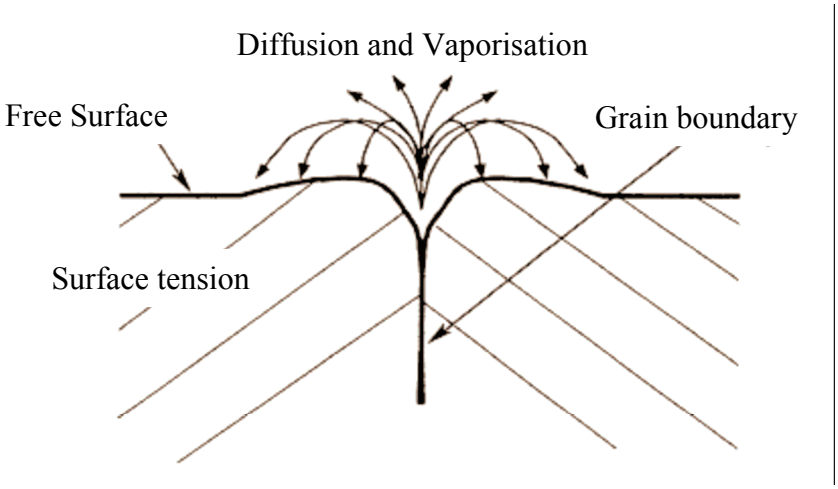

Figure 2. 3. The schematic image of the thermal etching method for revealing grain boundary. [2.12], [2.13], [2.14]

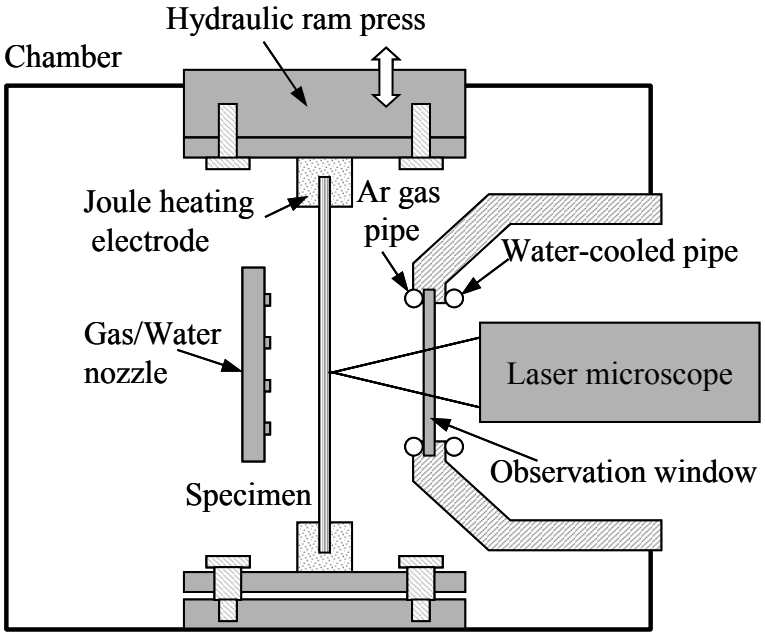

Figure 2. 4. Schematic diagram of the observation device.

.

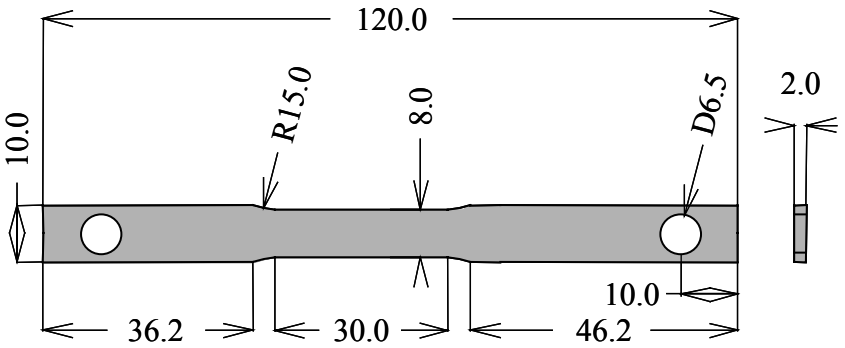

Figure 2. 5. The specimen for observation.

(Dimensions are mm.)

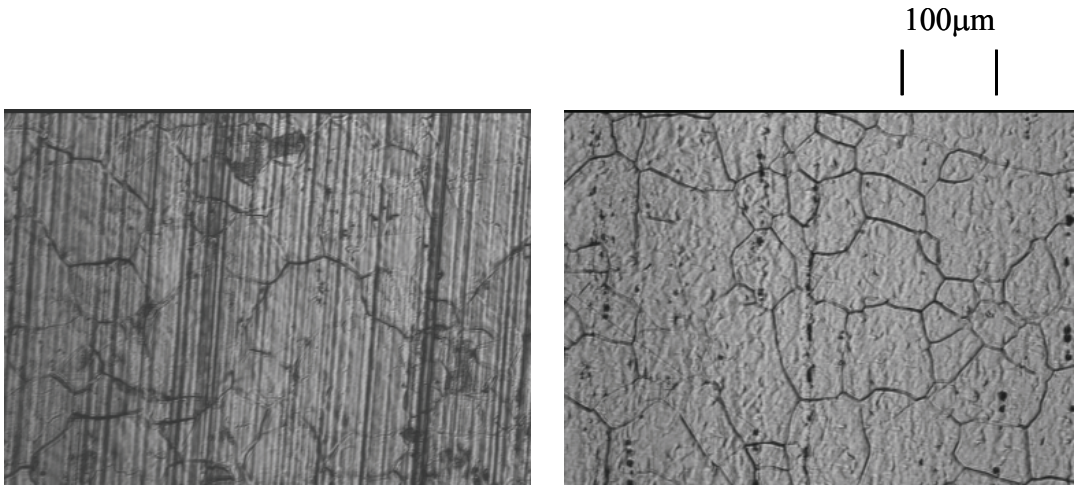

(a) Surface roughness: Rz = 0.2 ~ 0.3 μm (b) Surface roughness: Rz = 0.1 μm

Figure 2. 6. The difference of observed images depending on surface roughness.

2. 5. Experimental procedure

Observations of austenite structure were performed using the proposed observation device in order to confirm that austenite grain boundaries and their dynamic changes at high temperature can be observed using the proposed device. The specimen was the same as that in Figure 2. 5, and the material was S 25 C. The specimen was first heated to the observation temperature (1,373 K, 1,473 K, and 1,523 K) at a rate of 5 K/s, and then maintained at this temperature for 10 min. *In-situ* observation was carried out while maintaining the temperature, and observed image data were recorded at 15 Hz. Figure 2. 7 shows the experimental procedure using the new observation device.

The quantifying of grain size for the observed images were carried out by two methods depending on the objective. The first method was a liner intercept method to quantify average data for many grains. The second method uses image processing to quantify grain size for each of the specified grains. The image processing method can calculate the area of a grain, and the grain diameter is converted by the square root of grain area. The quantification of the grain sizes of the specified grains is one of the most important features of the new observation device.

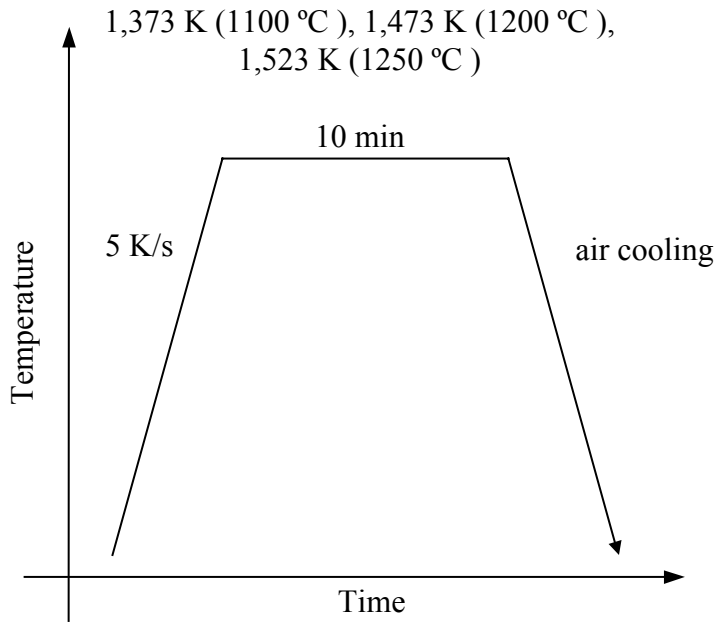

Figure 2. 7. Experimental procedure with the new observation device.

2. 6. Results and discussion

Figure 2. 8 through Figure 2. 11 show the changes of grain size at 1,523 K (1450°C), 1,473 K (1200°C), and 1,373 K (1100°C), respectively. These figures show that the new observation device can reveal grain boundaries and their dynamic changes at high temperatures. In order to easily identify microstructural changes, magnified images from Figure 2. 8 are shown in Figure 2. 9. The rectangle area in Figure 2. 8(a) is magnified. Arrows in Figure 2. 9 help readers to identify particular boundary movements.

Figure 2. 12 through Figure 2. 14 show the average grain size and the sizes of specified grains. The specified grains, which are selected randomly, are shown in Figure 2. 8 (a), Figure 2. 10 (a) and Figure 2. 11 (a). The grain sizes quantified by the conventional method are also plotted in the figures. Concerning the conventional method, the experiments were carried out by the following procedure (Figure 2. 15). The specimen was a cylindrical shape with a height of 12.0 mm and a diameter of 8.0 mm. The specimen was heated by induction heating to the observation temperature (1,373 K, 1,473 K, and 1,523 K) at a rate of 5 K/s and was maintained at the observation temperature for 1 minute and for 5 minutes, respectively. The specimen was then quenched in water to stop grain growth. The linear intercept method was applied to the quenched specimen to quantify the average grain size. Both the average grain size of the new observation method and that of the conventional method show good correspondence. Using the thermal etching method, it is expected that time be required for the primary grain boundaries to disappear and to reveal the new grain boundaries.

However, the correspondence of average grain size between the new observation device and the conventional method indicates that the velocity of the thermal etching method can follow the velocity of grain rearrangement in *in-situ* observation. The good correspondence also shows that the difference between the surface energy on a specimen surface and that in a specimen do not strongly influence grain growth of the austenite.

The average grain size, at each temperature, increases gradually, even though the size of some of the specified grains increase or decrease drastically with time. These drastic grain size changes indicate shrinking and expansion of grains. The feature of the *in-situ* observation method, that makes it possible to observe the grain size change of the same specimen in real time, is also able to analyze the shrinking and expansion of grains in greater detail.

The grain size changes, in more than two hundred of the grains, at 1,523 K were quantified by image processing, and a histogram of the grain size range and the frequency was generated (Figure 2. 16). Figure 2. 16 does not contain the error derived from the difference in initial structure because only one specimen was used for the observation.

From Figure 2. 16, the frequency under 40 μm decreases drastically, whereas the frequency over 100 μm increases gradually. In general, smaller grains have higher internal pressure. Therefore, in order to lower the Gibbs free energy, smaller grains would shrink, while neighboring larger grains would expand. This phenomenon is

explained by the Gibbs-Thomson effect. Figure 2. 16 supports the existence of this phenomenon.

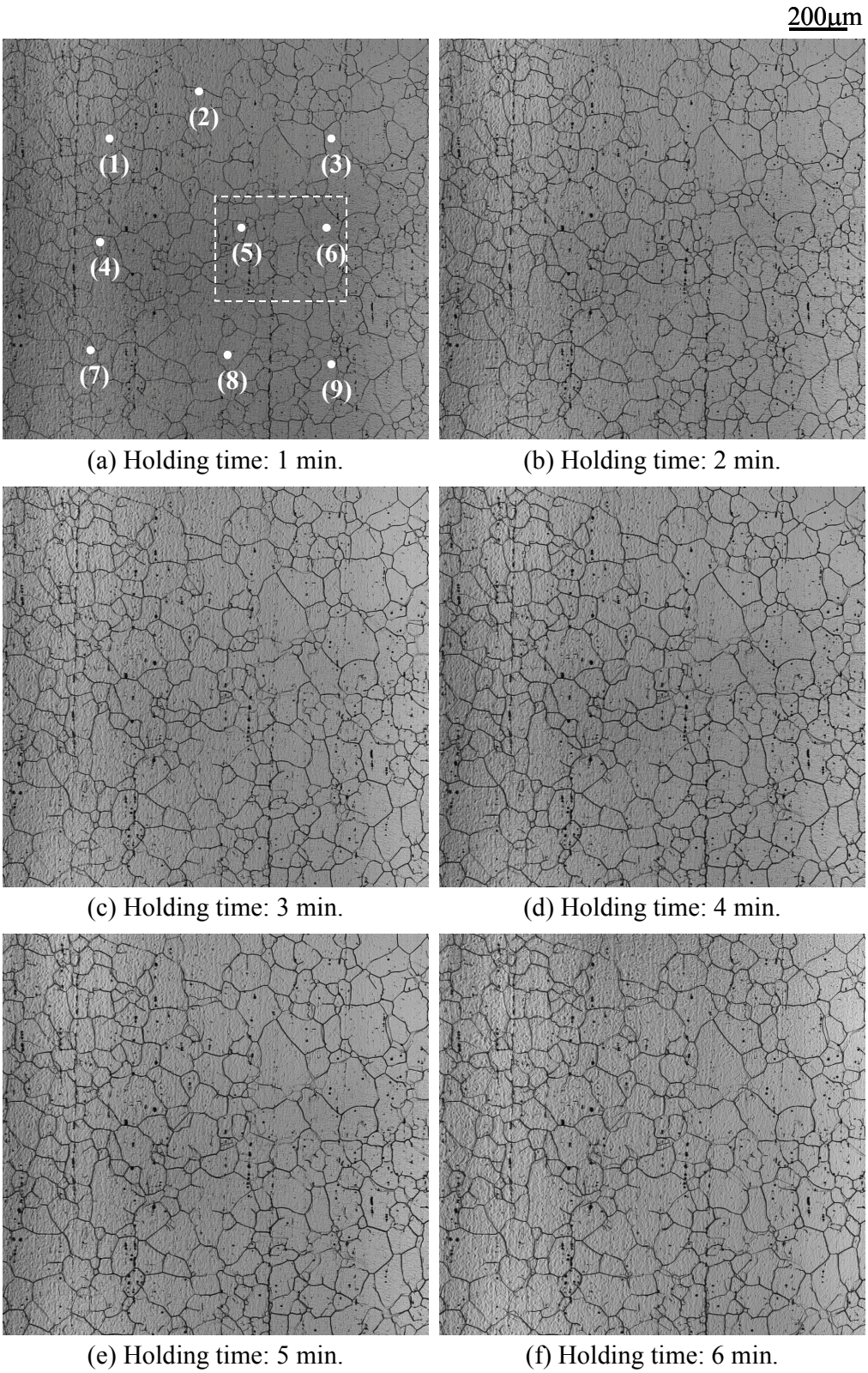

(a) Holding time: 1 min. (b) Holding time: 2 min.

(c) Holding time: 3 min. (d) Holding time: 4 min.

(e) Holding time: 5 min. (f) Holding time: 6 min.

Figure 2. 8. *Continued on the next page.*

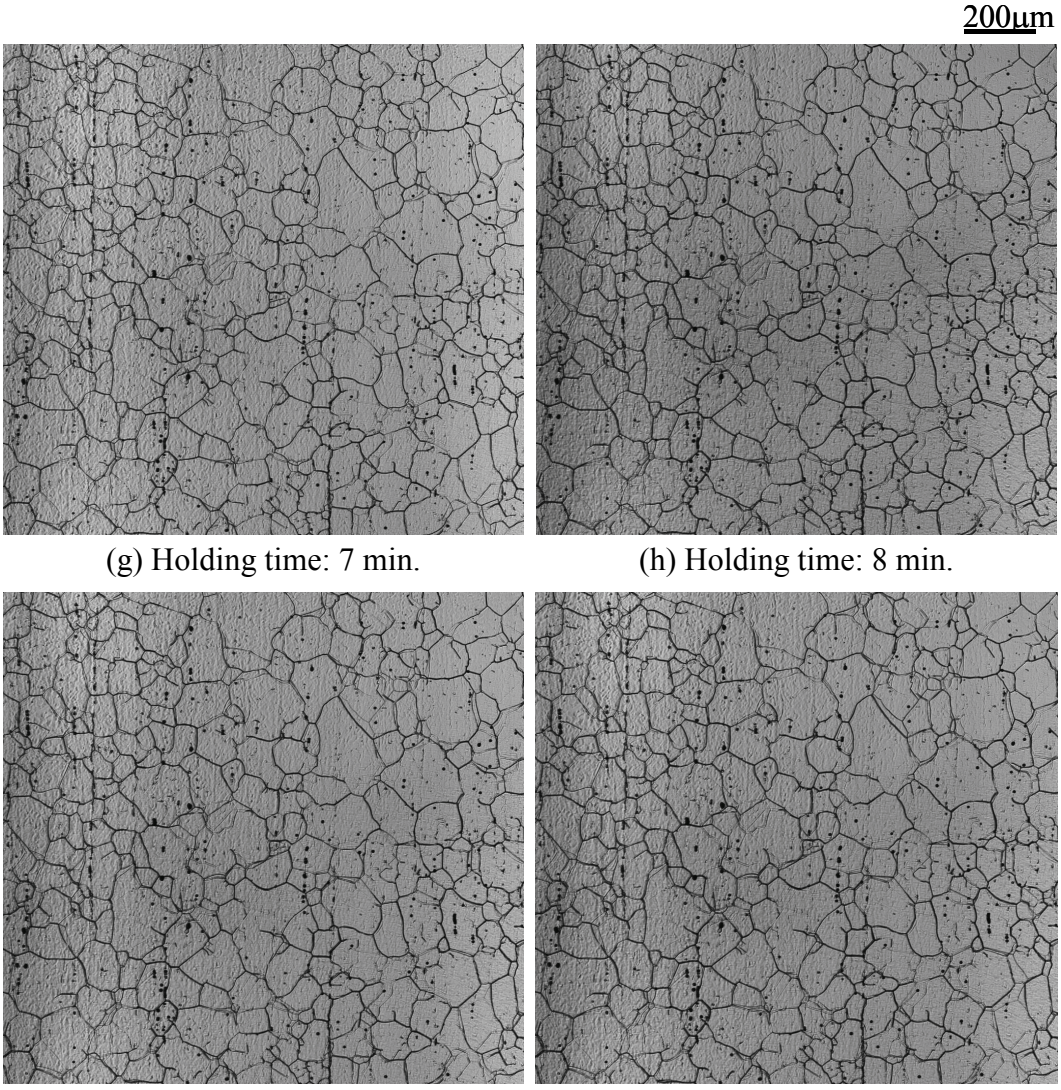

(g) Holding time: 7 min. (h) Holding time: 8 min.

(i) Holding time: 9 min. (j) Holding time: 10 min.

Figure 2. 8. Images of grain growth at 1523 K (1250°C).

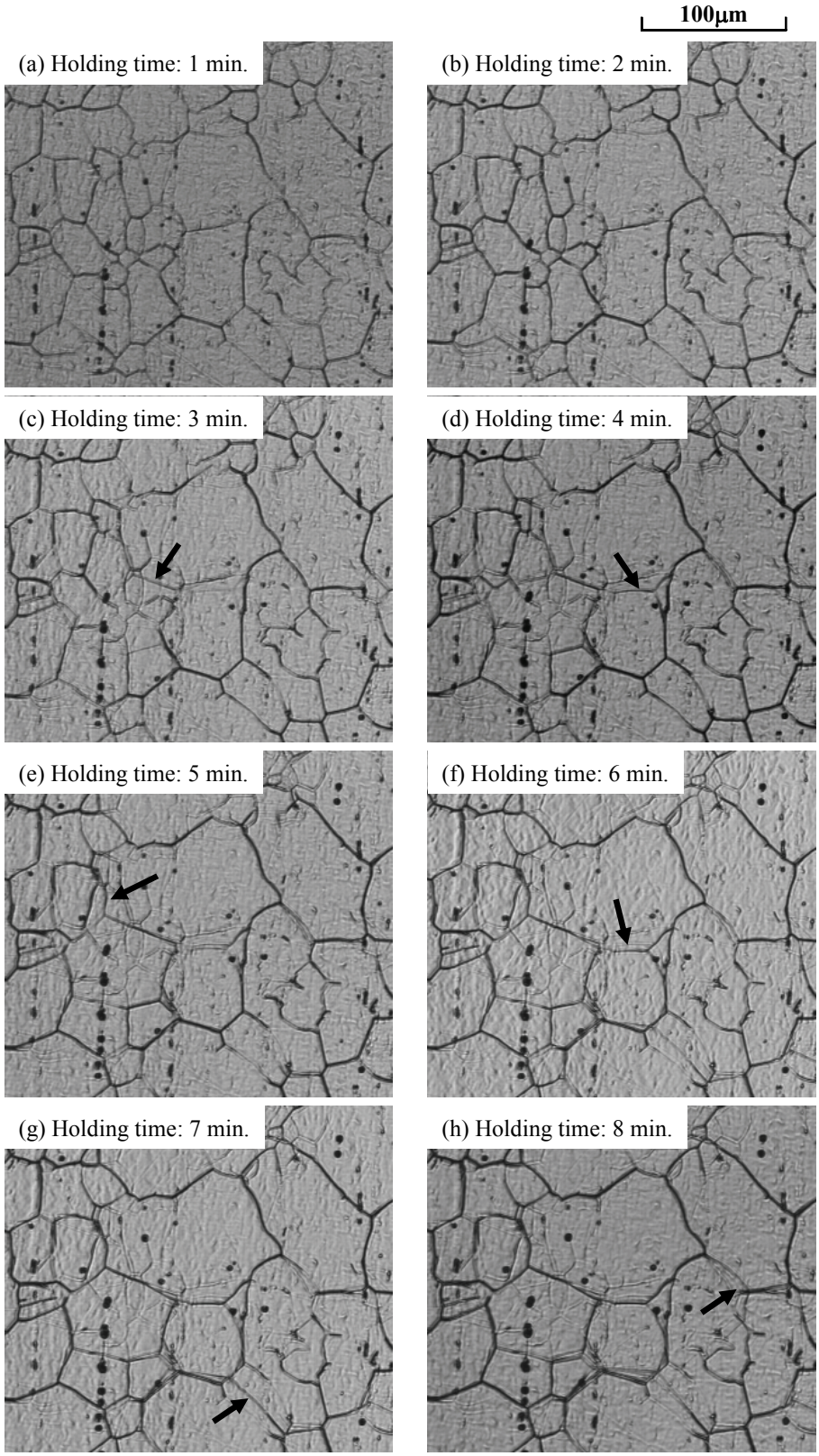

Figure 2. 9. Boundary movements during grain growth at 1523 K (1250°C).

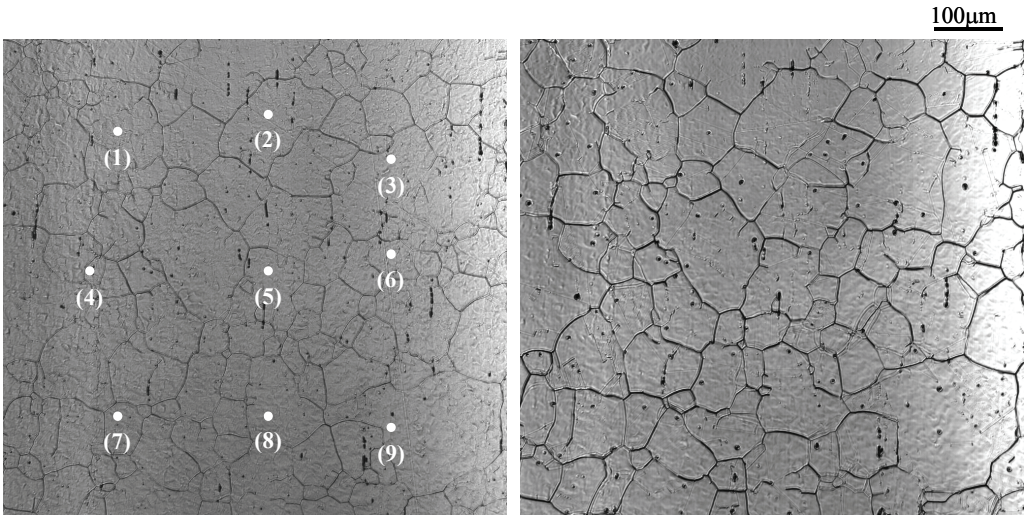

(a) Holding time: 1 min.

(b) Holding time: 10 min.

Figure 2. 10. Images of grain growth at 1473 K (1200°C).

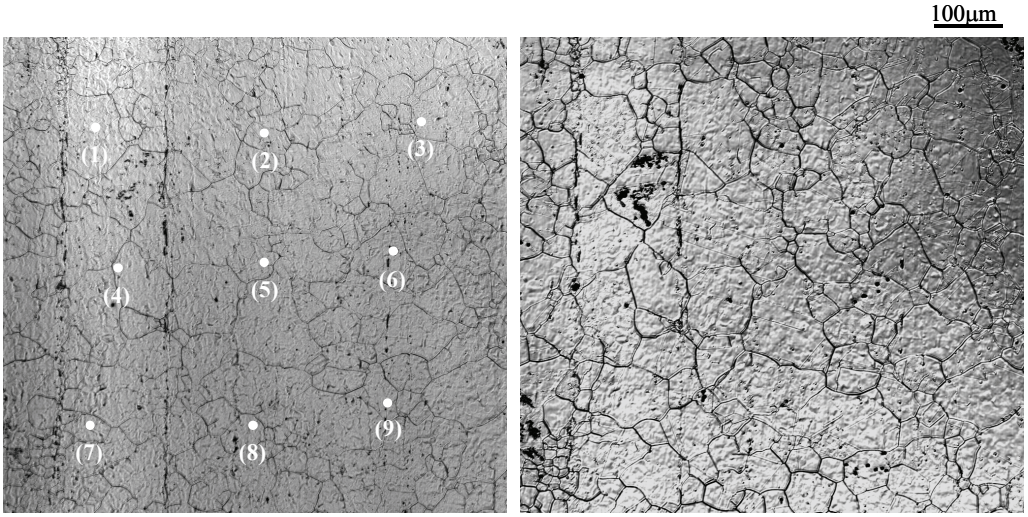

(a) Holding time: 1 min.

(b) Holding time: 10 min.

Figure 2. 11. Images of grain growth at 1373 K (1100°C).

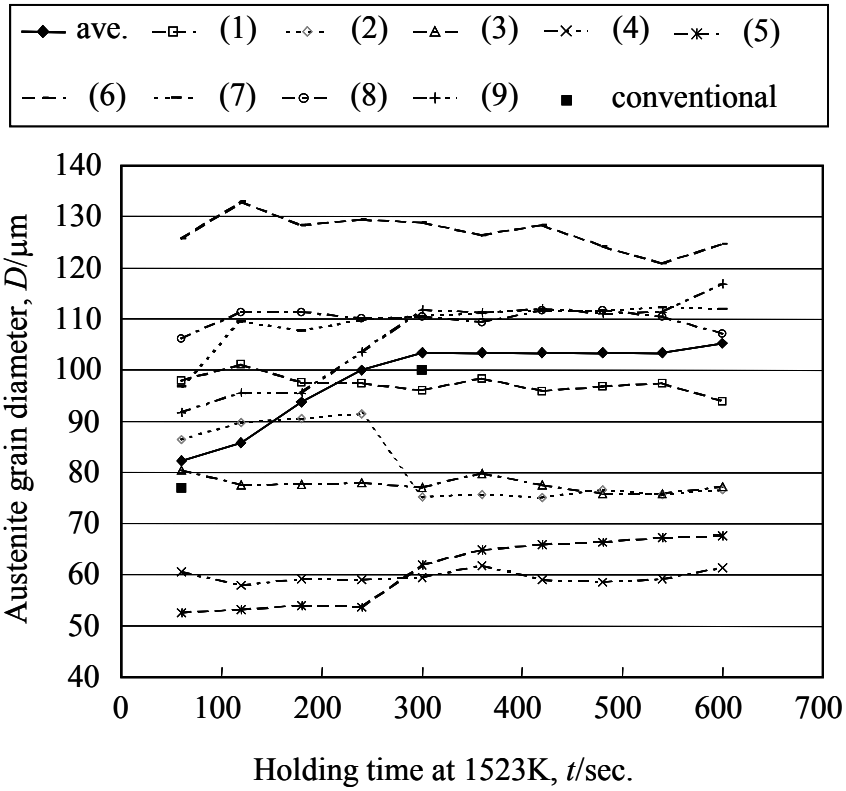

Figure 2. 12. Grain size change at 1523 K.

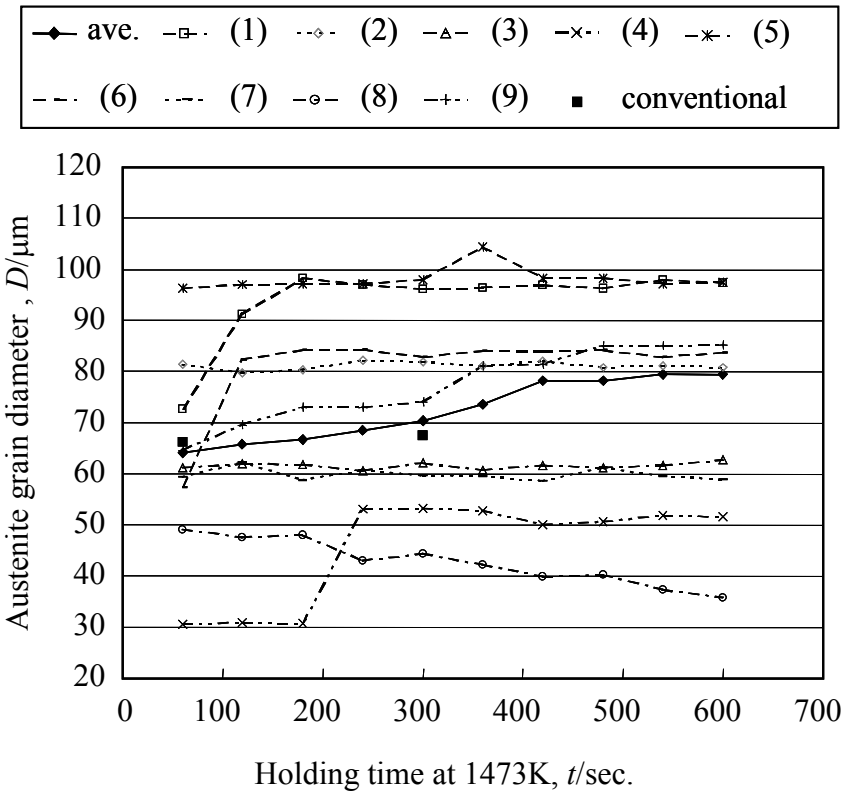

Figure 2. 13. Grain size change at 1473 K.

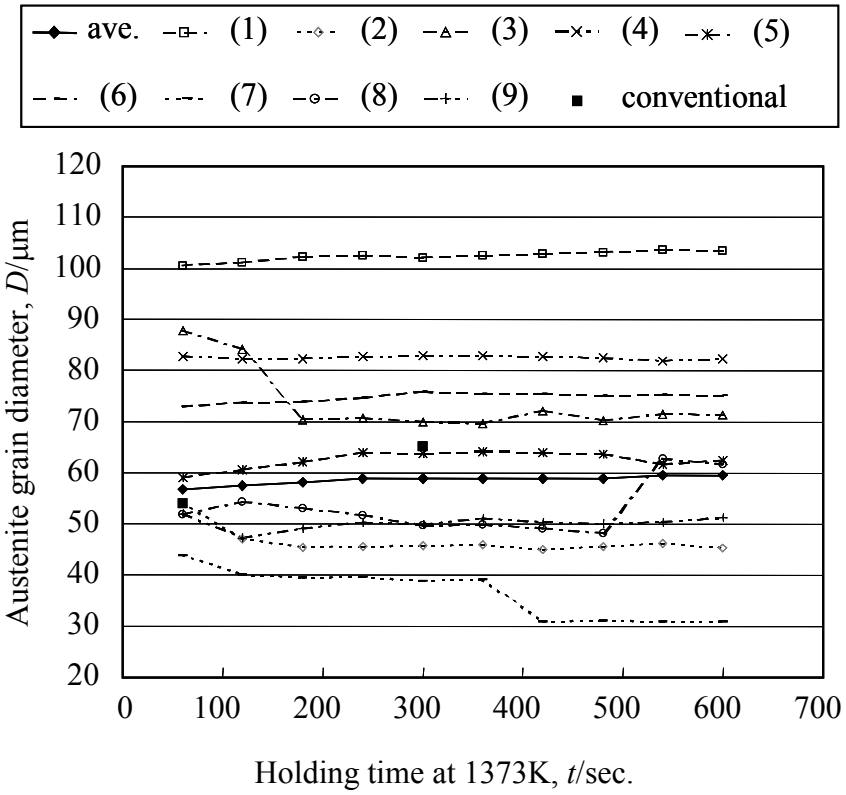

Figure 2. 14. Grain size change at 1373 K.

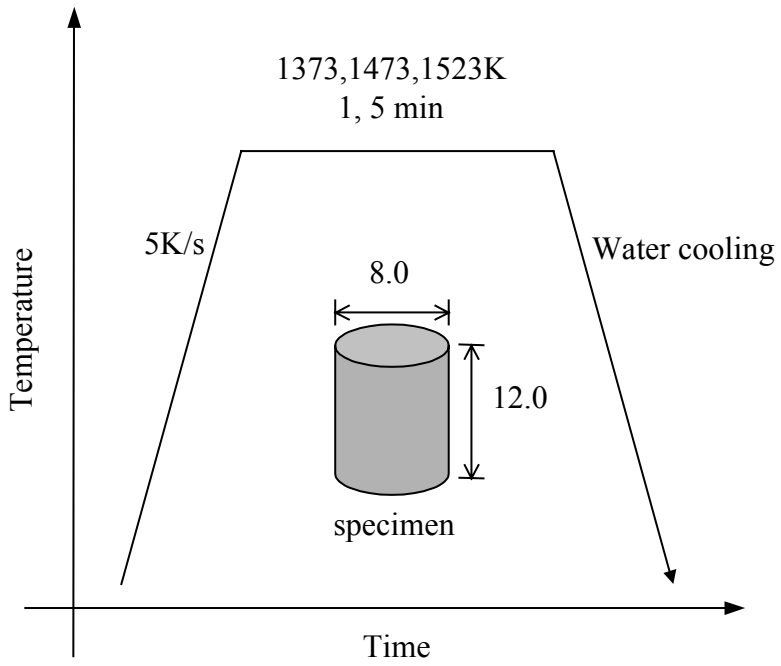

Figure 2. 15. The conventional experimental procedure.

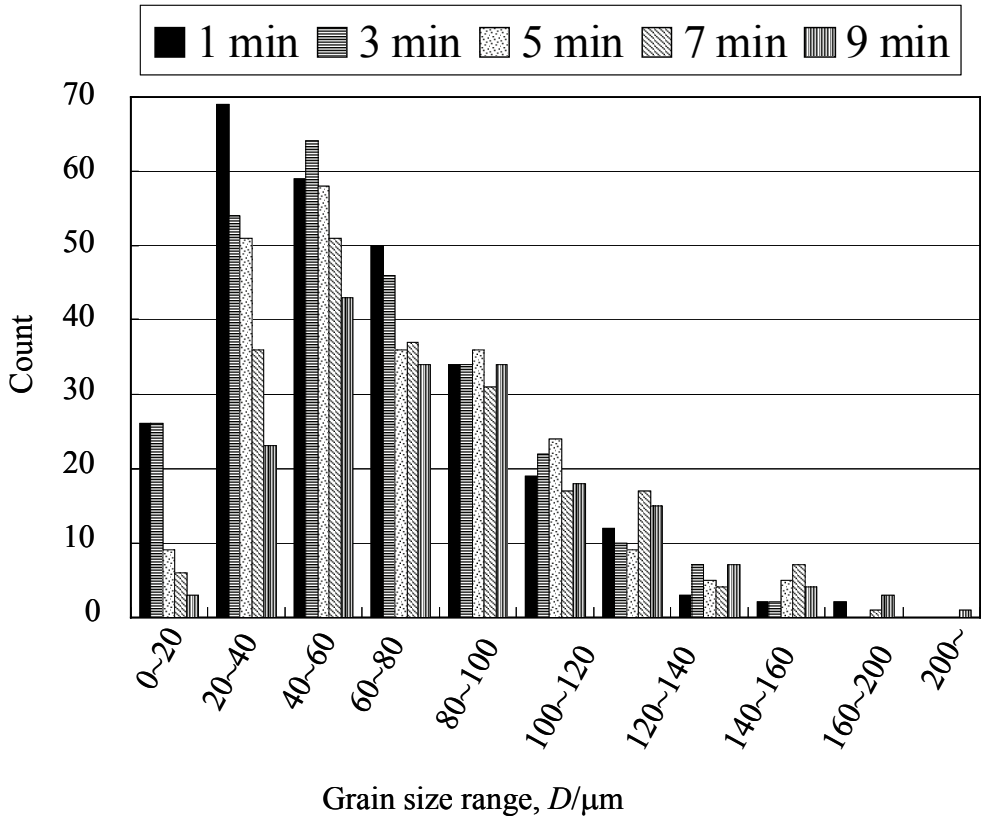

Figure 2. 16. Grain size histogram at 1523 K.

2. 7. Conclusions

A new observation device to observe microstructures at high temperatures was developed. Grain growth at high temperatures was observed by the new observation device. The average grain size and the grain sizes of specified grains were quantified. The tendency for smaller grains to be absorbed by neighboring larger grains is shown by the detailed data of quantified grain sizes.

These results demonstrate the effectiveness of the new observation device for observing microstructures at high temperatures. Moreover, the observed images, free from errors due to differences in the initial structures of specimens at each quantification, have great potential to quantify the grain size more precisely than the conventional method.

2. 8. Acknowledgements

The author would like to express his gratitude to M. Ikeda (Fuji Electronic Industrial Co., Ltd.) and M. Nakamura (Lasertec Corporation). Their cooperation was extremely helpful in developing the new observation device.

Reference

[2.1] C. M. Sellars and J.A. Whiteman: Met. Sci., 13 (1979), 187-194.

[2.2] John H. Beynon and C. Michael Sellars: ISIJ Int., 32 (1992), 359-367.

[2.3] T. Senuma, H. Yada, Y. Matsumura and T.Futamura: Tetsu to Hagane, 15 (1984), 2112-2119. (in Japanese)

[2.4] H. Yoshida, Y. Isogawa, Y. Kaneko, Y. Yogo and T. Ishikawa: J. JSTP, 43 (2002), 619-623. (in Japanese)

[2.5] H. Yoshida, Y. Isogawa, Y. Kaneko, Y. Yogo and T. Ishikawa: J. JSTP, 43 (2002), 973-977. (in Japanese)

[2.6] L. V. Azaroff, (1974). X-ray diffraction. McGraw-Hill.

[2.7] Yu-ichi Komizo and Hidenori Terasaki,Materials Science Forum, 638-642(2010) p3722-3726

[2.8] Klaus-Dieter Liss, Thomas Schmoelzer, Kun Yan, Mark Reid, Matthew Peel,Rian Dippenaar and Helmut Clemens, JOURNAL OF APPLIED PHYSICS 106,(200) 113526

[2.9] Seiichi Suzuki, Materia Japan, 40 (2001), pp. 612 － 616 (in Japanese)

[2.10] N.Takata, K.Ikeda, H.Nakashima: 151th. ISIJ meeting, 14th young scientist forum, 2006. (in Japanese)

[2.11] Pawley JB (editor) (2006). Handbook of Biological Confocal Microscopy (3rd ed.). Berlin: Springer.

[2.12] Mullins WW.: J. Appl. Phys., 27 (1957), 333-339

[2.13] Mullins WW.: Acta. Metall., 6 (1958), 414-427

[2.14] C. Garcia de Andres, F. G. Caballero, C. Capdevila and D San Martin: Matar. Charact., 49 (2003), 121-127

Chapter 3:

In-situ observation of SIBM during small hot deformation

3. 1. Background

Recrystallization has been one of the main topics of focus for researchers for the last several decades due to the fact that the fine grains produced by recrystallization are desirable for industrial-use steel parts. Therefore, elementary mechanisms of recrystallization have been investigated in conventional experiments and the results have been well documented. [3.1], [3.2]

While there are many research results for recrystallization under large strains, recrystallization under small strains has not been as thoroughly investigated. This is due to the limitations of conventional experimental methods. For the purpose of the investigation into the dynamic recrystallization (DRX) of carbon steel, flow stress has been focused. [3.3], [3.4] As DRX is somewhat of a restoration process, the occurrence of DRX influences flow stress. The rapid cooling method using water or He gas to cool a specimen immediately after hot deformation to stop microstructural changes has also been applied. [3.5], [3.6] As a result of this, observations of microstructural changes during DRX and static recrystallization were conducted on specimens whereby the microstructural changes were halted by rapid cooling. These two conventional methods can be applied when investigating recrystallization under large strains. However, the

investigation of microstructural changes over small strains range are difficult with these two methods. This is due to the fact that over the small strain range at which DRX does not appear, microstructures do not change drastically and the changes occur very locally. Therefore, flow stress is not strongly influenced by slight microstructural changes, and slight microstructural changes are difficult to identify through the observation of cooled specimens using the rapid cooling method.

As a result of the above-mentioned difficulties, microstructural changes during strain under the critical strain of DRX have not been researched extensively, in particular for carbon steel. Therefore, there are few results which have focused on microstructural changes under small strains. [3.7], [3.8], [3.9], [3.10] In such experiments, the existence of grain coarsening phenomena under small strains and the conditions under which they occur were discovered. However, microstructural phenomena caused by small strains were not studied.

3. 2. Purpose of this study

The *in-situ* observation method [3.11], [3.12] proposed in chapter 1 is first applied to observations during small strains at high temperatures and, then the investigation of microstructural changes are conducted under small strains. This research discusses the microstructural changes, such as strain induced boundary migration (SIBM), of a carbon steel during small strains at high temperatures. Through the investigation by the *in-situ* observation method, the rate of SIBM and the SIBM initiating strain is measured.

3. 3. Experimental procedure

In order to observe microstructural changes of carbon steel deformed under small strains at high temperatures, the *in-situ* observation method developed in chapter 1 was applied. The schematic diagram of the system is shown in Figure 2.4. The specimen dimensions are shown in Figure 2.5. The material used was S25C (Fe - 0.22 mass% C- 0.19 mass% Si - 0.51 mass% Mn). A specimen was first heated to 1273 K, 1373 K and 1473 K by Joule heating at 5 K/s, and then held at that temperature for two minutes. The specimen was then deformed in tension over 20.0% at 1.0mm/min, during which time the *in-situ* observations were made and observed images recorded at 15 frames per second. Having been recorded as movie files, the observation and measurement of microstructural changes was possible. During the *in-situ* observation, the distance of the ram movement was also recorded. As a result, the strain of the observed images can be easily measured by the recorded distance.

It was expected that microstructural changes during small strains would be observed locally. Therefore, in order to obtain an average for the dispersion of each specimen, five specimens were used in each experimental condition.

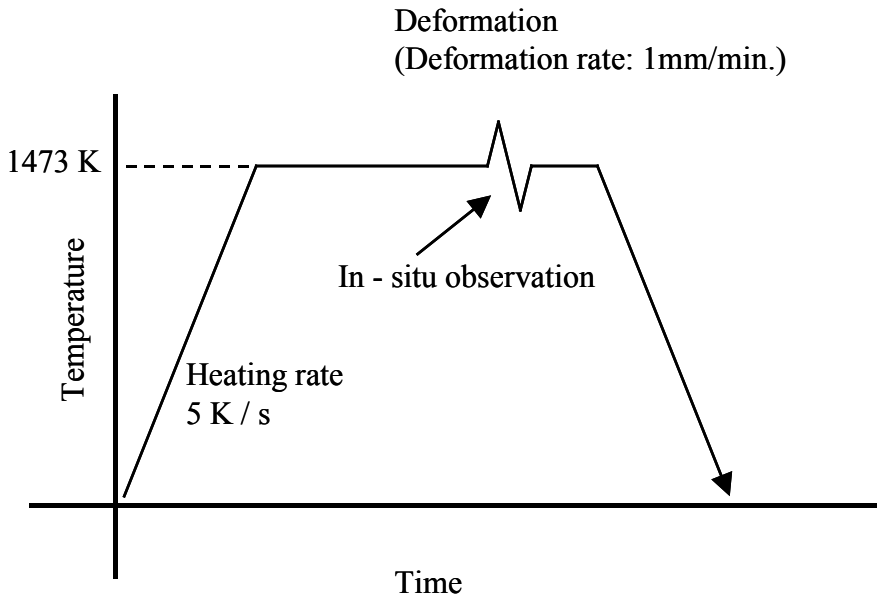

Figure 3. 1. Thermal and mechanical history.

3. 4. Results and discussion

According to the observed images, the critical strain for DRX was measured first. In this study, the strain at which a new boundary appears from the initial microstructure is defined as the critical strain for DRX. Determining the critical strain for DRX is conducted by identifying the appearance of a new grain, which can be ascertained by viewing the recorded images of *in-situ* observations. As mentioned above, this determination method is more sensitive than the conventional method which relies on the identification of a flow stress curve. The temperature dependency of the critical strain for DRX is shown in Figure 3. 2. The calculated critical strain for DRX using Senuma's equation [3.13] is also plotted in Figure 3. 2. The critical strain for DRX decreases with rising temperatures. Experimental and calculated values show close correspondence at 1373 K and 1473 K. The reason for the discrepancy between experimental and calculated values at 1273 K would be derived from the difference of sensitivity between observation methods. Senuma et al. [3.13] developed the equation by calculating statistics of observed results of water cooled specimens by the rapid cooling method. The calculated DRX fraction at 1273 K by the equations is not high, which means DRX appears locally at 1273 K. Therefore, the identification of DRX from other structures in water cooled specimens is not easy to attain. As a result of this, the critical strain for DRX determined by water cooled specimens has a tendency to be larger than the actual value. On the other hand, the *in-situ* observation method enables the observation of the exact time when DRX appears. As such, the critical strain for DRX of the experiments by the *in-situ* observation method would be smaller than the calculated one.

During small strains under the critical strain for DRX, SIBMs were clearly observed by the *in-situ* observation method. Representative SIBM forms observed at 1473 K are shown in Figure 3. 3. It is confirmed through observations that SIBM occur on flat boundaries and on concave and convex triple junctions.

The rate of SIBM was measured at each temperature. The histogram between SIBM rate and the relative frequency is shown in Figure 3. 4. The relative frequency was calculated at each of the three temperatures. Figure 3. 4 shows that much of SIBM occur at the rate of 0.2 to 0.6 μm/s, and the tendency at which the SIBM rate is higher at higher temperatures is recognized. According to the results in chapter 1, the rate of grain growth while maintaining a temperature of 1473 K without deformation is slower than 0.1 μ m /s. Remarkably, the SIBM rate is at least ten times higher than the grain growth rate.

The driving force for grain growth is about 0.1 (J/mol). In the case of SIBM, the driving force derived from deformation should also be considered. The driving force derived from deformation can be estimated from the dislocation density using [3.14]

$$\Delta G_{tot} = \rho G b^2$$

Here, ρ is dislocation density, G is the shear modulus of Fe and b is the Burgers vector of dislocation. The dislocation density at the SIBM initiating strain can also be estimated as about 1.0×10^{13} (/m^2) [3.13]. Using the dislocation density, the driving force of SIBM is estimated about 1.0 (J/mol). The driving force is dissipated by the solute drag effect during grain boundary movement. By plotting both the driving force for

grain growth and SIBM into Figure 6.8, it is shown that the relationship between the dissipation energy by the solute drag effect during grain boundary movement and velocity of grain boundary movement (Figure 3. 5). It is acceptable that the application of small strains such as the SIBM initiating strain makes grain growth rate ten times faster than that for grain growth without deformation. (Detailed discussions of the driving force of grain growth and Figure 6.8 will be shown in chapter 6.)

The SIBM initiating strain at each temperature is shown in Figure 3. 6. It is confirmed that SIBM was initiated by even such small strains as 0.015. This value is smaller by an order of magnitude than the critical strain for DRX (Figure 3. 2).

$$\varepsilon_c = 4.76 \cdot 10^{-4} \exp\left(\frac{8000}{T}\right) \quad [3.13]$$

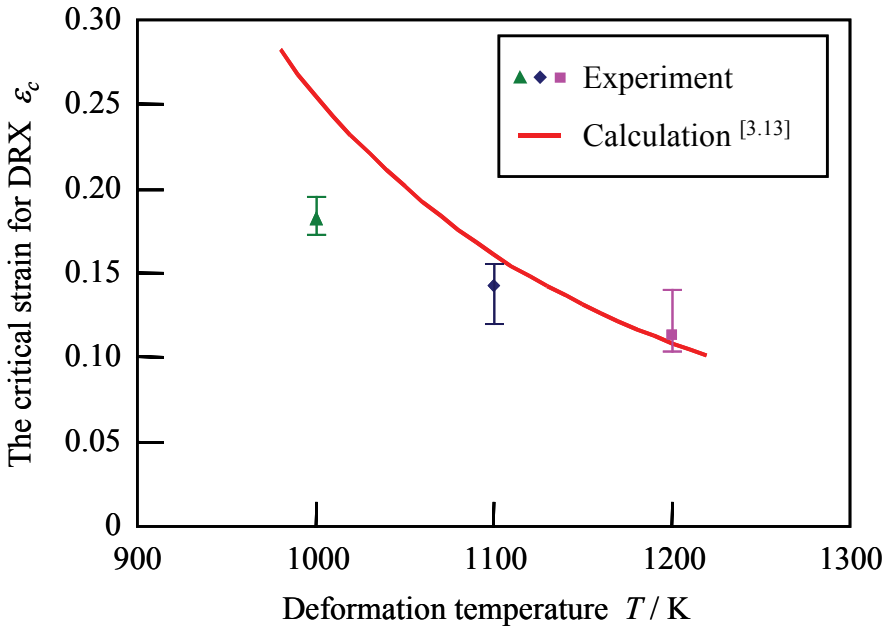

Figure 3. 2. The critical strain for DRX.

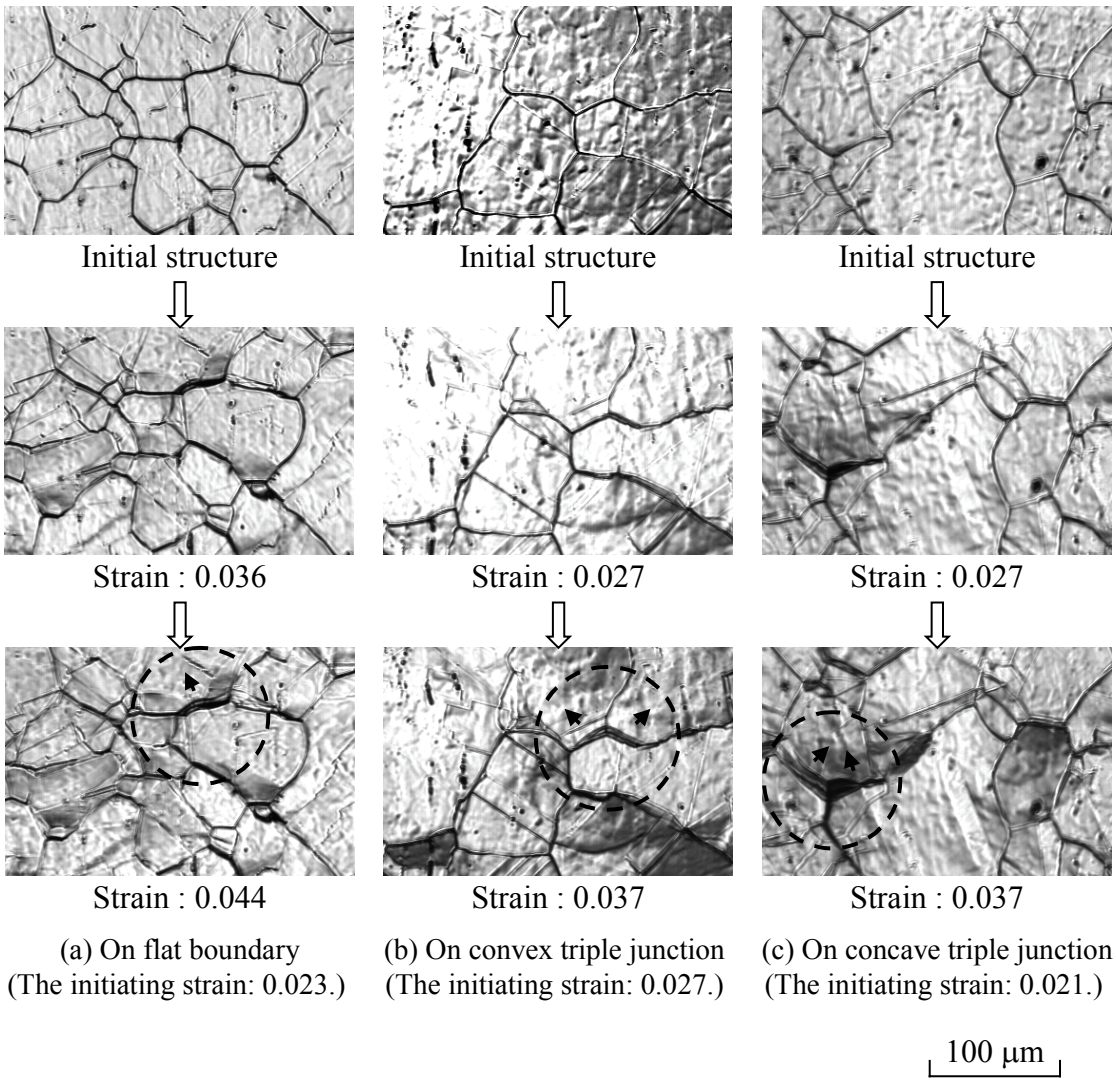

Figure 3. 3. Representative forms of SIBMs at 1473 K.

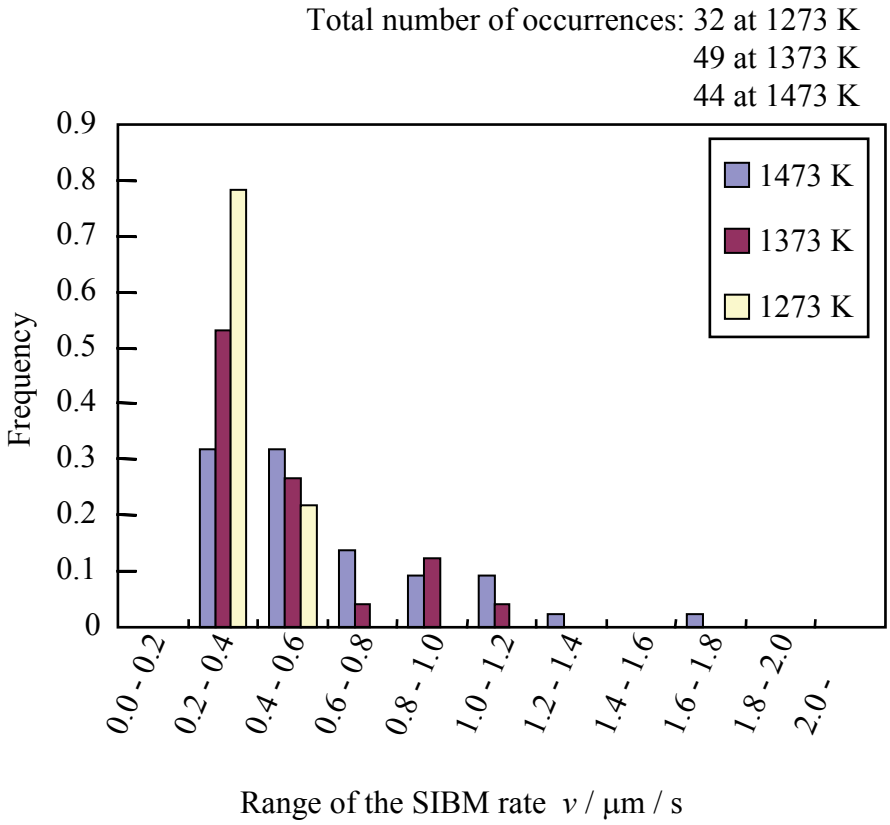

Figure 3. 4. The histogram of SIBM rate vs. frequency.

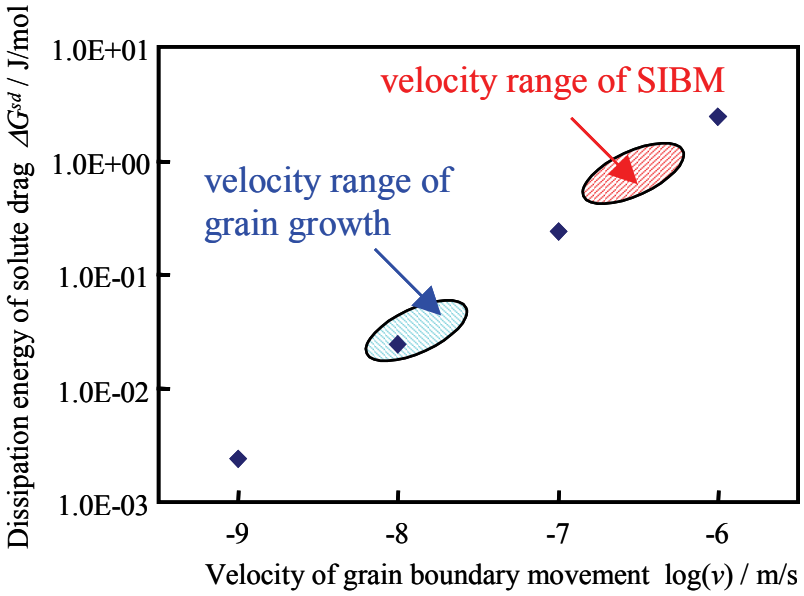

Figure 3. 5. The relationship between dissipation energy and velocity during grain boundary movement.

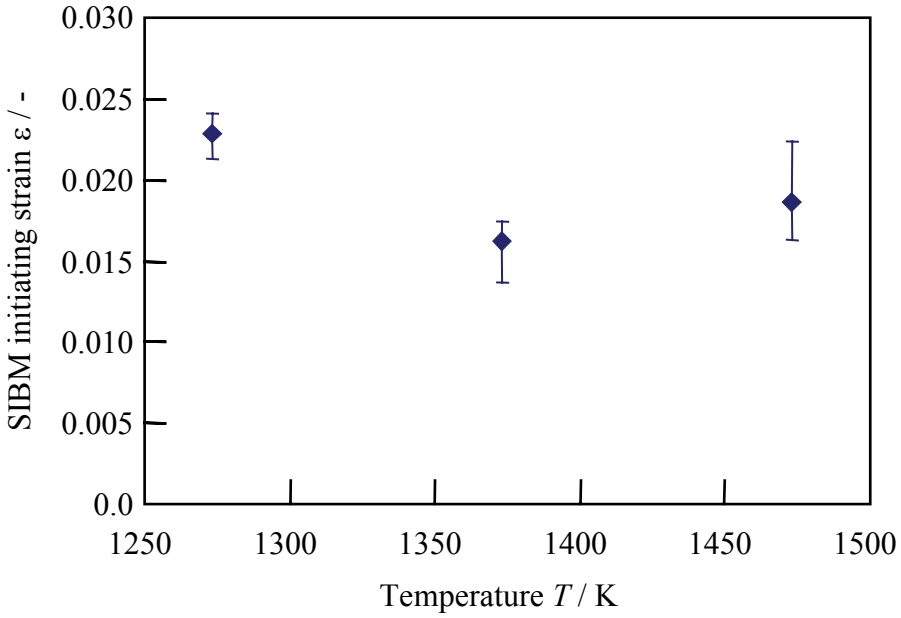

Figure 3. 6. The SIBM initiating strain.

3. 5. Conclusion

In this study, through the investigation of SIBM, it is confirmed that the developed *in-situ* observation method can be applied to observations during application of small strains at high temperatures. This investigation confirms that SIBM appears on various forms of grain boundaries. By the *in-situ* observation method, the rate of SIBM was successfully measured, and the rate of SIBM measured is much higher than the rate of grain growth without strain. It was confirmed that the SIBM initiating strain is smaller by an order of magnitude than the critical strain for DRX.

References

[3.1] F. J. Humphreys, M. Hatherly. Recrystallization and Related Annealing Phenomena Second edition, Elsevier, Oxford, 2004.

[3.2] R. D. Doherty, D. A. Huges, F. J. Humphreys, J. J. Jonas, D. Juul Jensen, M. E. Kassner, W. E. King, T. R. McNelley, H. J. McQueen, A. D. Rollett. Mater. Sci. Eng., A238 (1997) pp. 219 - 274.

[3.3] M.J Luton, C.M Sellars. Acta. Metal., 17 (1969) pp. 1033 - 1043.

[3.4] M. Maki, I. Tamura. Materia Jpn., 19 (1980) pp. 59 - 63. (in Japanese)

[3.5] H. Yada, N. Matuzu, K. Nakajima, K. Watanabe, H. Tokita. Trans. ISIJ, 23 (1983) pp. 100 - 109.

[3.6] H. Yada, N. Matuzu, Y. Matsumura, J. Tominaga. Tetsu-to-Hagane, 70 (1984) pp. 2128 - 2135 (in Japanese).

[3.7] G. A. Edwards, L. B. Pfeil. Iron Steel Inst., 190 (1924) pp. 129 - 147.

[3.8] Y. Neishi, M. Akiyama. Mater. Sci. Tech., 18 (2002) pp.799 - 803.

[3.9] Y. Neishi, M. Akiyama, Y. Inoue, K. Kawakami. J. Jpn. Soc. Tech. Plast., 38 (1997) pp. 637 - 641. (in Japanese)

[3.10] Y. Neishi, M. Akiyama, K. Kuroda. J. Jpn. Soc. Tech. Plast., 39 (1998) pp. 1134 - 1138. (in Japanese)

[3.11] Y. Yogo, K. Tanaka, K. Nakanishi. Mater. Trans., 50 (2009) pp. 280 - 285

[3.12] Y. Yogo, H. Takeuchi, K. Tanaka, N. Iwata, K. Nakanishi and T. Ishikawa. Microscopy Research and Technique, 72 (2009) pp.899–901.

[3.13] T. Senuma, H. Yada, Y. Matsumura, T. Futamura. Tetsu-to-Hagane, 70 (1984) pp. 2112 - 2118. (in Japanese)

[3.14] M. Suehiro: ISIJ Int., 38 (1998), p. 547-552.

Chapter 4:

In-situ observation of dynamic recrystallization

4. 1. Background

The microstructure of steel can be changed by various different mechanisms: phase transformation, recrystallization or grain growth during thermomechanical or heat treatment processes. In order to observe such changes, a specimen is usually quenched from high temperature to room temperature using water or He gas to stop the microstructural changes and allow for observation at room temperature [4.1] . Although this is a very useful experimental method to determine the tendencies of microstructural changes, this method does not give accurate information about when and where the observed phenomena start to occur, and can only infer what phenomena have occurred at high temperatures from the quenched microstructures. In recent developments, two remarkable observations of microstructural changes of steel at high temperatures have been reported. The first one reported observation results of static recrystallization of interstitial free (IF) steel up to 1073 K using electron back scattering pattern (EBSP) [4.2]. The other observed grain growth of plain carbon steel up to 1523 K using a confocal scanning violet laser microscope [4.3]. These observation methods significantly expanded the temperature range in which microstructural changes at high temperatures can be observed. However, in both studies *in-situ* observation were not carried out during large deformation.

4. 2. Purpose of this study

In the case of hot deformation of steel, microstructural changes caused by hot deformation over 1173 K, such as recrystallization, are often used to produce high quality industrial parts [4.4], [4.5]. Therefore, it is important to observe and understand microstructural changes during deformation at high temperatures. In the chapter 3, the developed *in-situ* observation method was applied to observe microstructural changes, SIBM, under small strains at high temperatures. In this chapter, the developed *in-situ* observation method is applied to observations for dynamic recrystallization which appears under a condition of hot large deformation.

4. 3. Experiment and results

The observation device used is shown in Figure 2.4 and specimen dimensions are shown in Figure 2.5. The experiment was carried out using the following procedure (Figure 4. 1). A specimen was first heated to 1473 K by Joule heating at 5 K/s and then held at this temperature for two minutes. The specimen was then tensile strained to 22.4% at the rate of 0.25mm/min. *In-situ* observations were made during this process and images were recorded at 15 frames per second. During the *in-situ* observation, the distance of the ram movement is also recorded, so the strain of observed images can be measured from the recorded distance. The observation results are shown in Figure 4. 2. Increasing strain, a new grain boundary, which potentially could be a recrystallized

grain, appears. That grain is highlighted by dotted circle. The recrystallized grain then grows in the direction of the arrow.

In the following, using a higher powered objective lens, an observation was conducted by the procedure of Figure 4. 3. Figure 4. 4 (a) and (b) show the microstructure before and after deformation under strain to 22.4% respectively. The crosses are used as guide marks to identify the initial structure. Grain deformations are apparent by looking at the guide marks. The circled area in Figure 4. 4 (b) is magnified in Figure 4. 5 to highlight the microstructural changes. Under strain, curved lines as deformed structures, which potentially could be dislocation substructures, were spreading over the grain (Figure 4. 5 (a)). Figure 4. 5 (b) shows the appearance of a new grain boundary, potentially it could be a recrystallized grain boundary. Figure 4. 5 (c) and (d) show that the new grain boundary has a sweeping motion inside the grain. In the area where the new grain boundary is swept, the deformed structures disappeared. The disappearance of the deformed structures could be caused by the same mechanism as recrystallization.

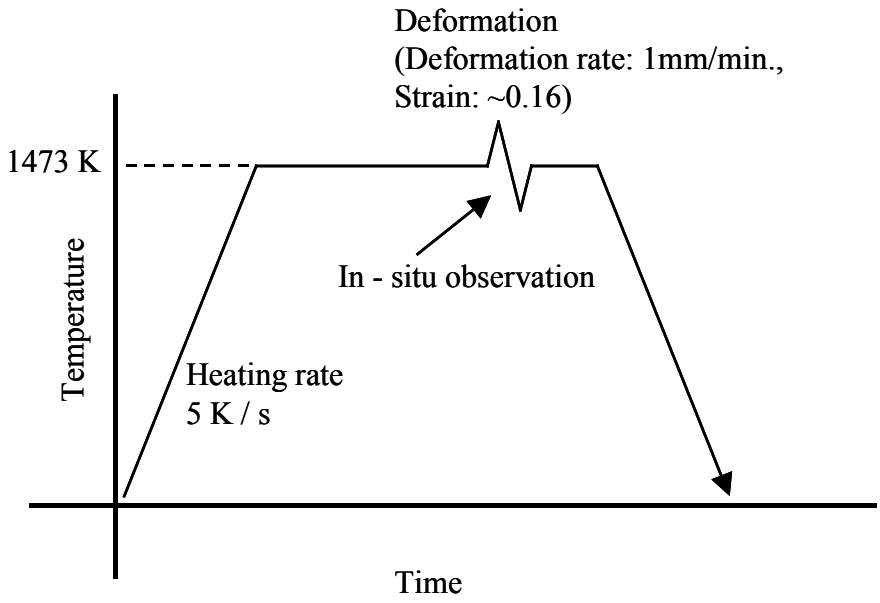

Figure 4. 1. Thermal and mechanical history.

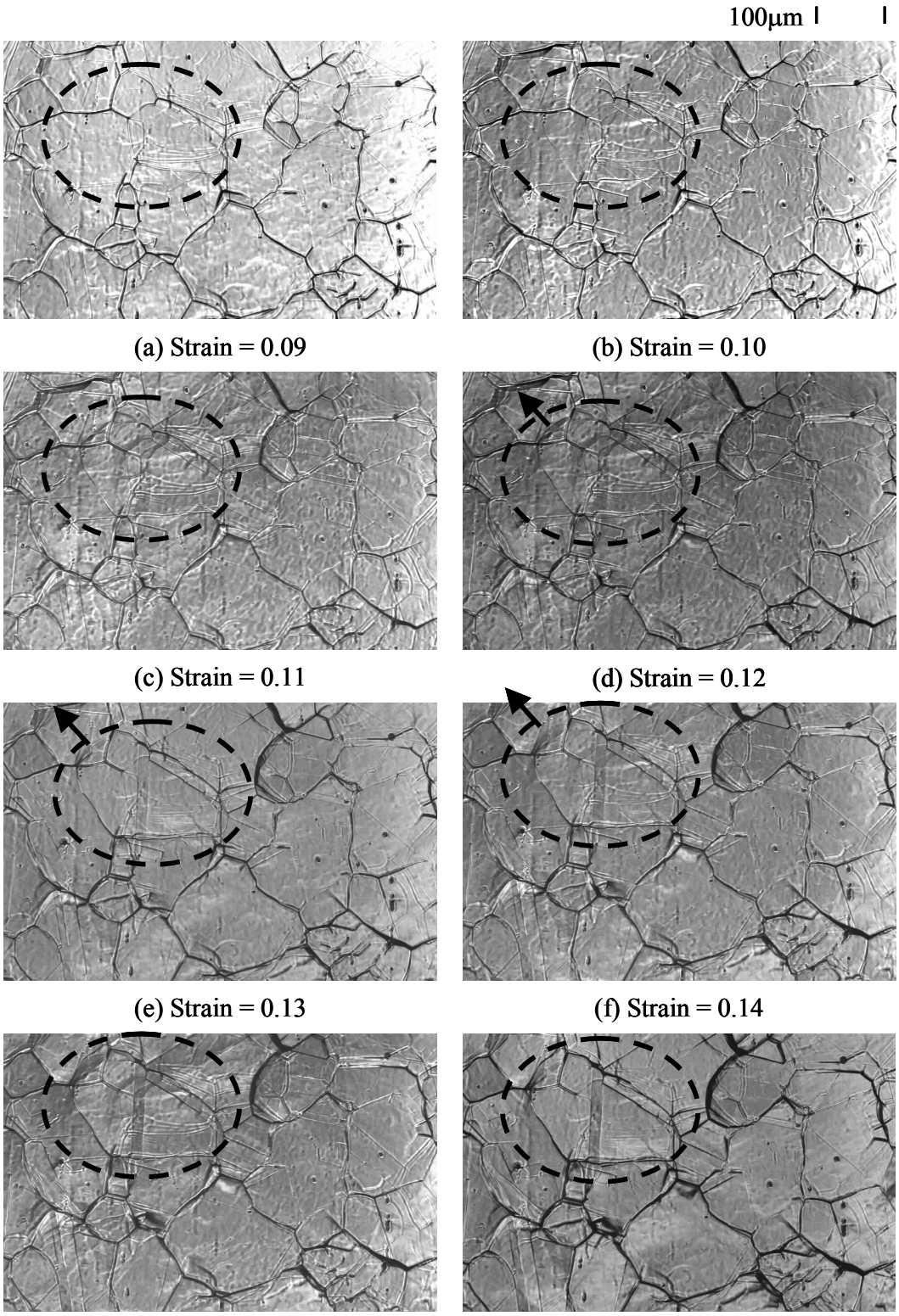

Figure 4. 2. Microstructural changes during hot deformation at 1473 K.

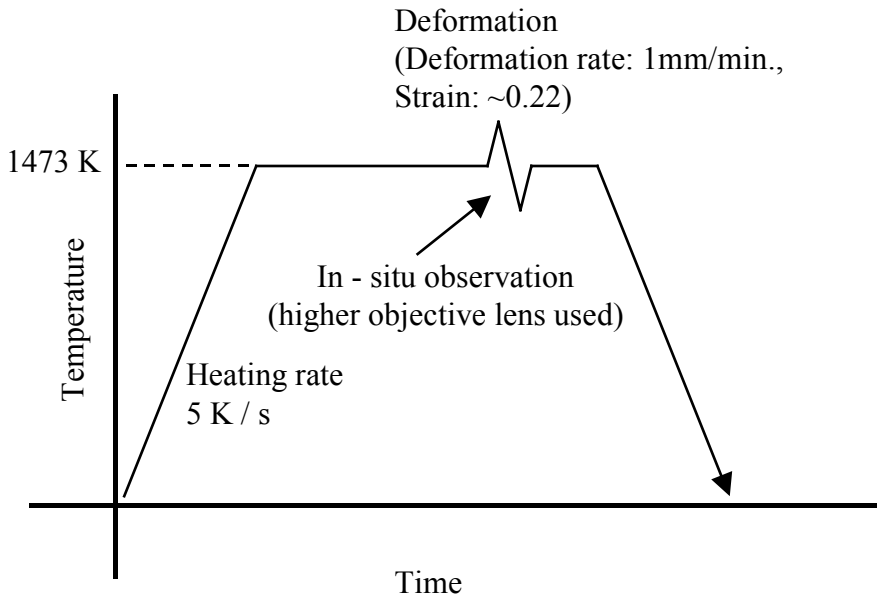

Figure 4. 3. Thermal and mechanical history.

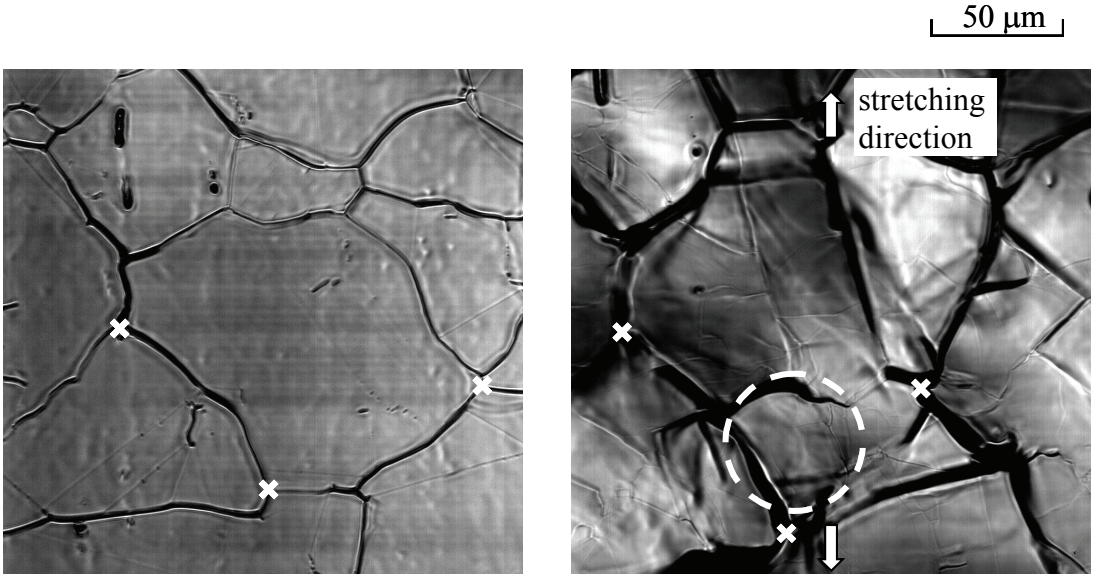

(a) before deformation (b) after deformation (strain: 22.4 %)

Figure 4. 4. Microstructural change under strain at 1473 K.

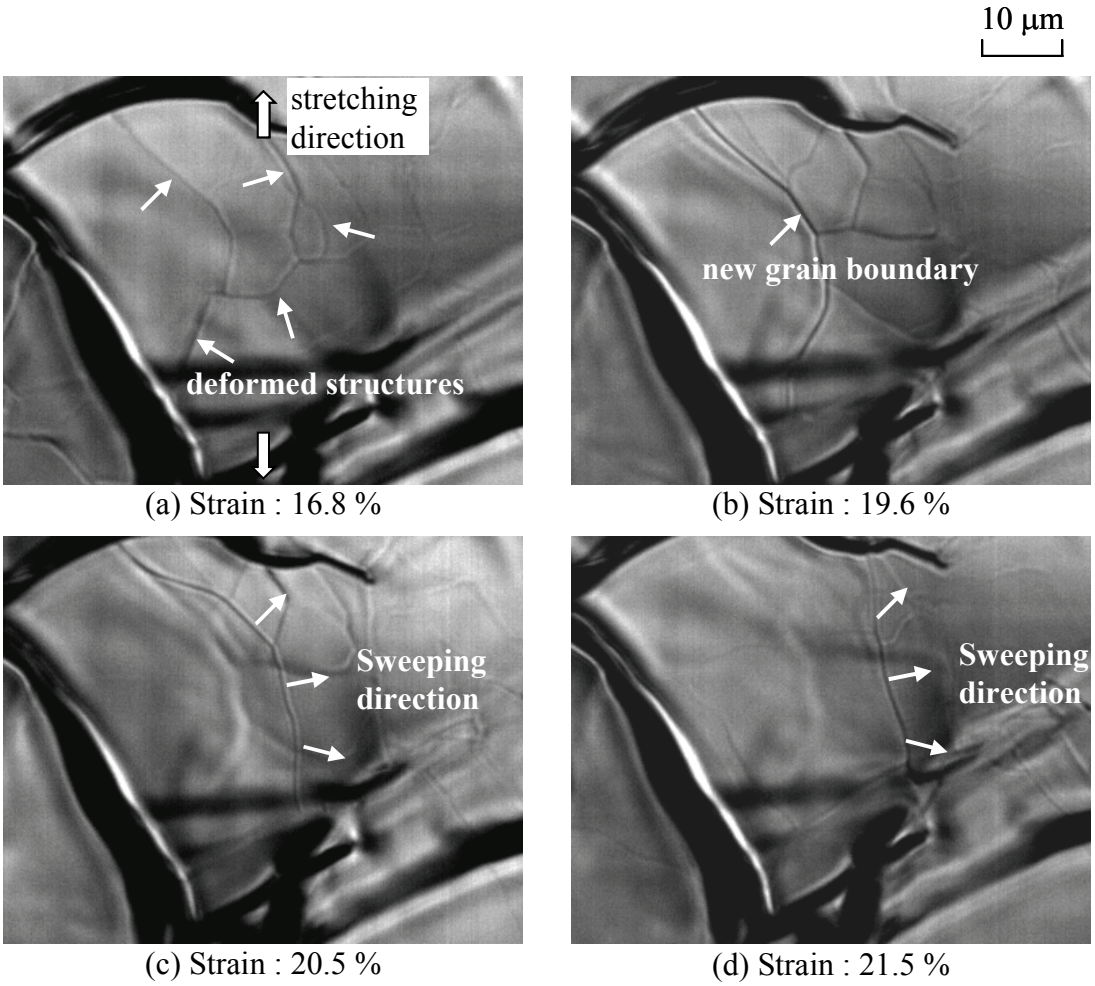

(a) Strain : 16.8 %

(b) Strain : 19.6 %

(c) Strain : 20.5 %

(d) Strain : 21.5 %

Figure 4. 5. Observations of deformed structures and the formation of a new grain boundary.

4. 4. Conclusion

By observing dynamic recrystallization, it is confirmed that the developed *in-situ* observation method can be applied to observations for microstructural changes during hot deformation. Images clearly show that the microstructural changes during hot deformation at 1473 K, which has until now been considered very difficult to observe, can now be recorded using the method reported here. This method is applicable to a wide range of microstructural observations at high temperature.

References

[4.1] H. Yada, N. Matsuzu, Y. Matsumura, J. Tominaga. Tetsu-to-Hagane , 70 (1984) pp. 2128-2135. (in Japanese)

[4.2] H. Nakamichi, F. J. Humphreys, I. Brough. J Microscopy, 230 (2008) pp. 464-471.

[4.3] Y. Yogo, K. Tanaka, K. Nakanishi. Mater Trans, 50 (2009) pp. 280-285.

[4.4] H. Yoshida, S. Isogawa, Y. Nakeko, Y. Yogo, T. Ishikawa. J of JSTP , 43 (2002) pp. 619-623.

[4.5] H. Yoshida, S. Isogawa, Y. Nakeko, Y. Yogo, T. Ishikawa. J of JSTP, 43 (2002) pp. 973-977.

Chapter 5:

In-situ observation of phase transformation during heating and cooling

5. 1. Purpose of this study

By using the developed *in-situ* observation method, (1) inverse phase transformation during heating from (ferrite and pearlite) to austenite, and (2) phase transformation during cooling from austenite to (ferrite and pearlite) can be observed. Following this, observed images by the *in-situ* observation method and the conventional method using an optical microscope are compared.

5. 2. Experimental procedure

The *in-situ* observation system is shown in Figure 2.4. The material S25C is applied for this experiment. A specimen dimension is shown in Figure 2.5. Thermal history for the *in-situ* observation is shown in Figure 5. 1. A specimen is heated at the rate of 1 K / s, and temperature is maintained at 1473 K (1200 ^{0}C), then the specimen is cooled down to 873 K (600 ^{0}C) at the rate of 5 K / s. During this thermal history, *in-situ* observation was conducted and digitally recorded as movie files.

In order to compare images of the *in-situ* observation method and the conventional method, the specimen, which cooled down to 873 K (600 ^{0}C), is quenched in water. Next, the specimen is polished to a mirrored surface, etched by Nital acid, and finally observed with an optical microscope.

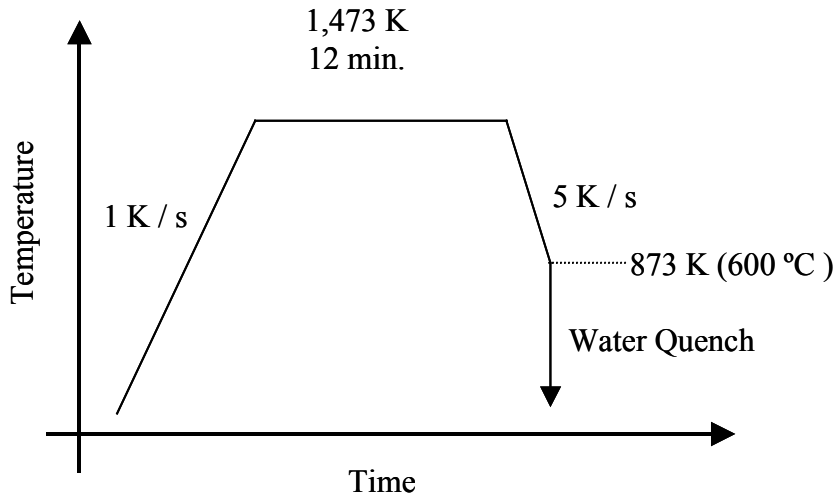

Figure 5. 1. Thermal history for observing phase transformation.

5. 3. Observed images and discussion

5. 3. 1. Observed images during heating

Observed images during heating process are shown in Figure 5. 2. These images are captured from the observation movie at every 200 K. While heating up, a specimen expands due to thermal expansion. To observe the same position throughout the entire observation period, the position of the laser microscope is adjusted with the specimen's thermal expansion. The image of (a) at 873 K (600 ^{0}C) does not show anything. This is because temperature is not high enough to activate thermal etching. However, from the images of (b) to (d), the change of microstructure from ferrite and pearlite to austenite can be recognized.

According to Fe - C binary phase diagram shown in Figure 5. 3, the A_1 temperature is about 1000 K (727 ^{0}C). In order to look specifically for the appearance of the austenite, images around the A_1 temperature are captured in Figure 5. 4. It is difficult to identify the appearance of the austenite by looking at those captured images. In the following images at 1313 K (1040 ^{0}C), 1333 K (1060 ^{0}C), 1353 K (1080 ^{0}C) and 1373 K (1100 ^{0}C) are captured and shown in Figure 5. 5. In this temperature range, it is possible to observe appearance of the austenite. It is natural that the microstructural changes from (the ferrite and the pearlite) to the austenite in the temperature range between the A_1 and the A_3 temperatures always occur. However, by using the *in-situ* observation method, temperature at which appearance of the austenite was observed is much higher than A_1 temperature. Investigation into the mechanism during inverse

phase transformation is one of the hottest research themes. Therefore, improvement of the observation method to apply to inverse phase transformation would be a future challenge.

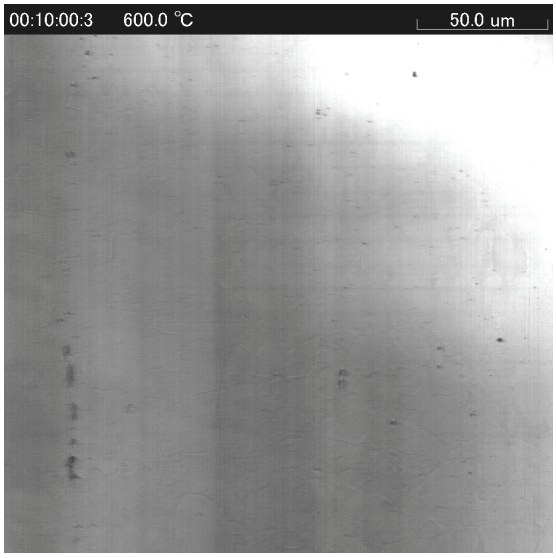

(a) 873 K (600 ºC)

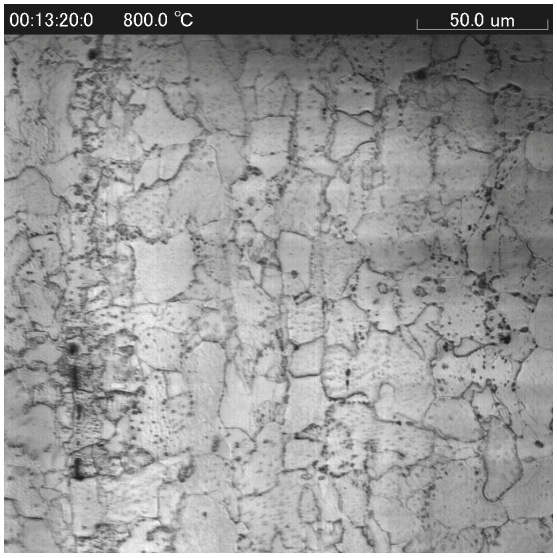

(b) 1073 K (800 ºC)

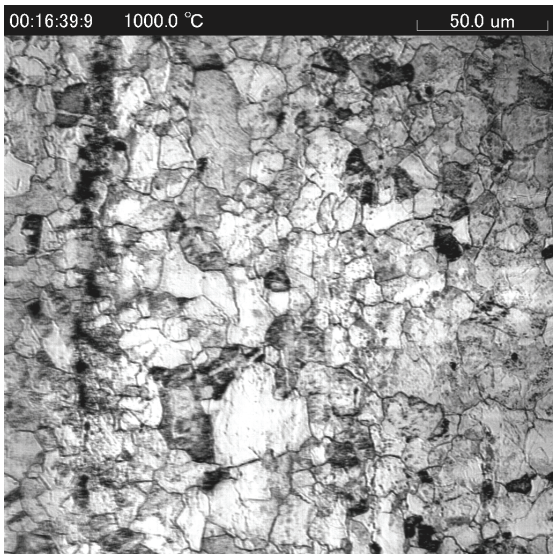

(c) 1273 K (1000 ºC)

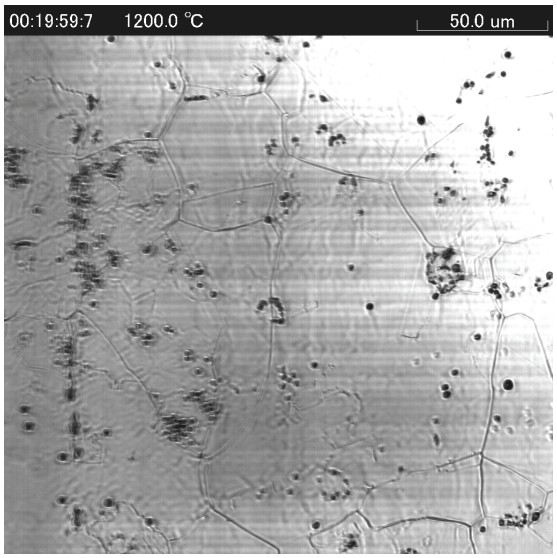

(b) 1473 K (1200 ºC)

Figure 5. 2. Observed images during heating.

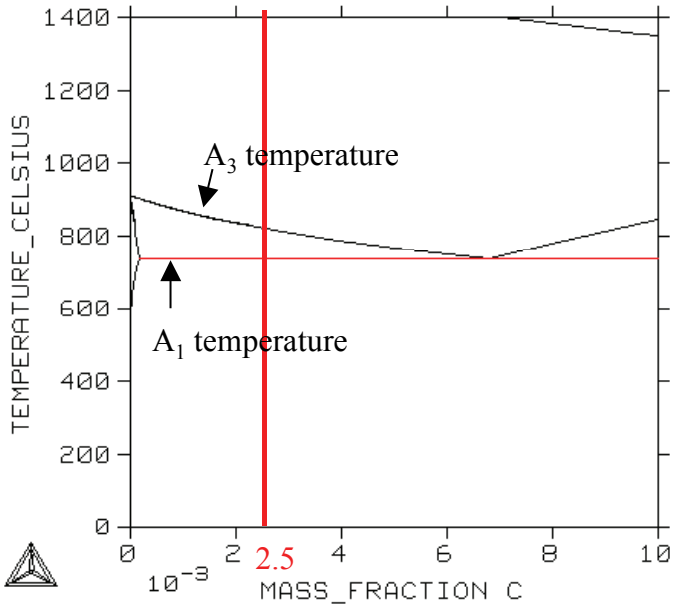

Figure 5. 3. Fe-C binary phase diagram.

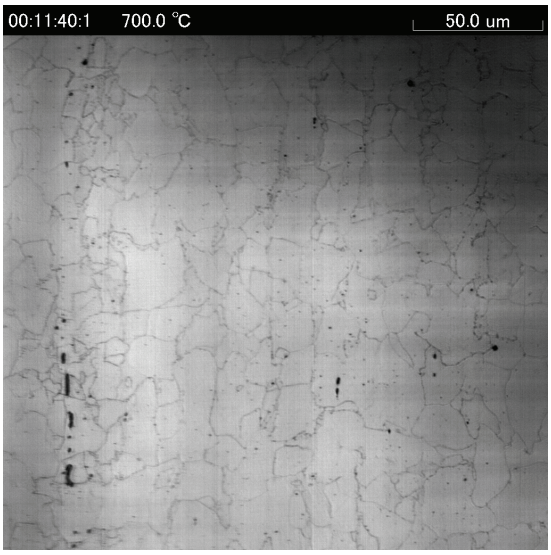

(a) 973 K (700 ºC)

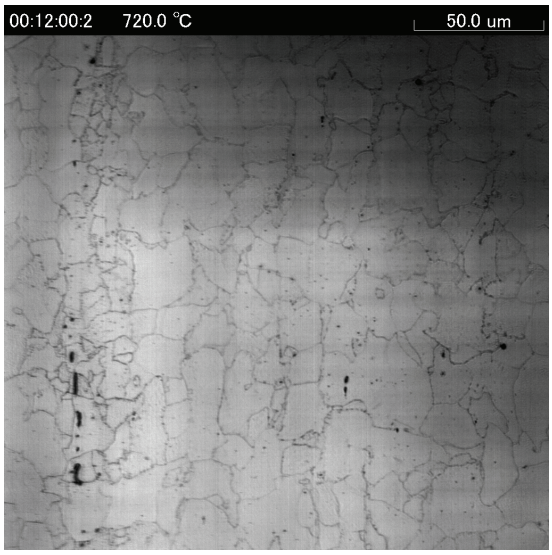

(b) 993 K (720 ºC)

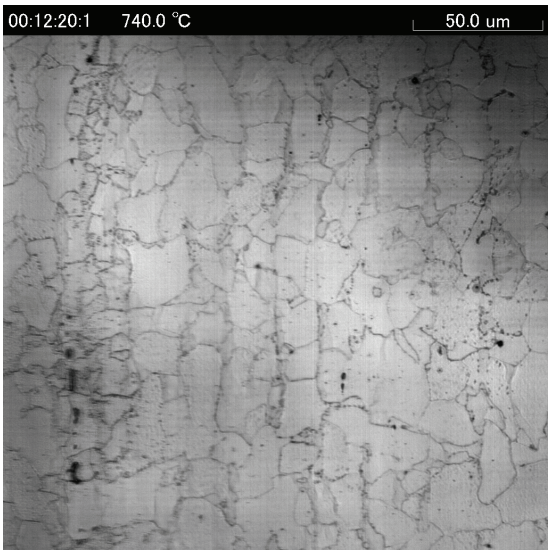

(c) 1013 K (740 ºC)

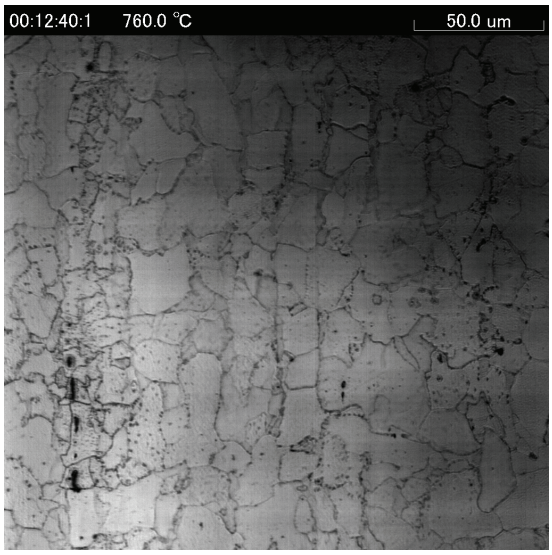

(d) 1033 K (760 ºC)

Figure 5. 4. Observed images around A_1 temperature.

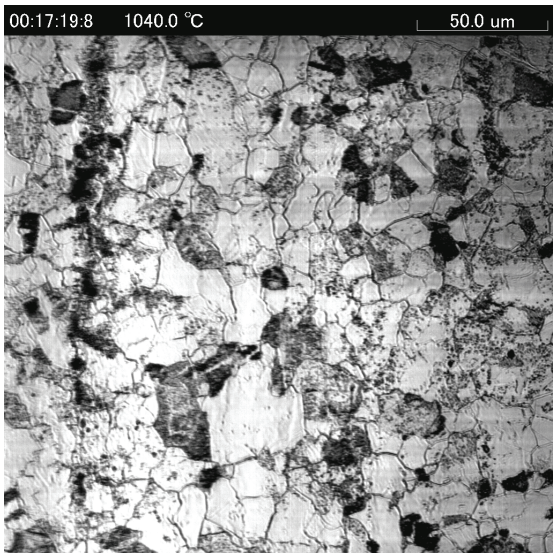

(a) 1313 K (1040 ºC)

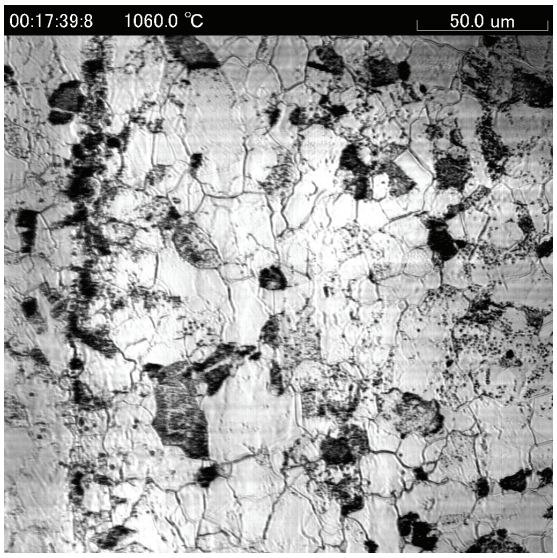

(b) 1333 K (1060 ºC)

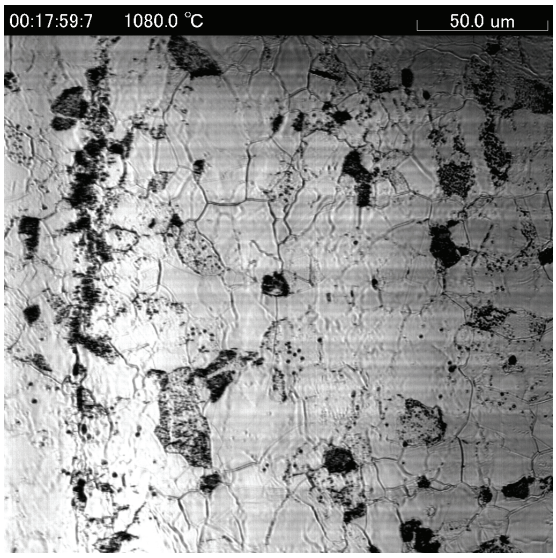

(a) 1353 K (1080 ºC)

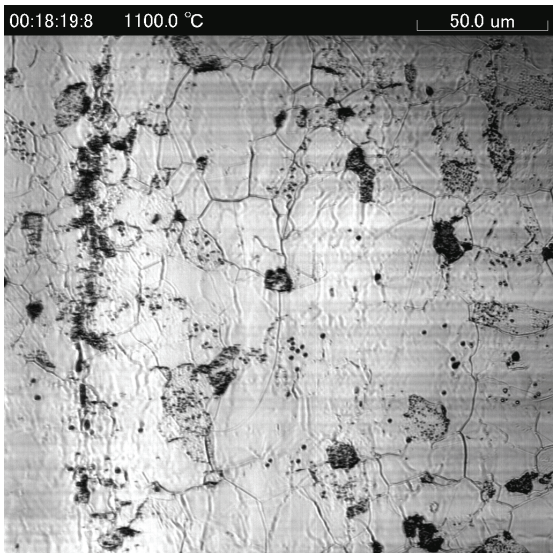

(b) 1373 K (1100 ºC)

Figure 5. 5. Appearance of austenite.

5. 3. 2. Observed images while maintaining temperature at 1473 K

While maintaining temperature at 1473 K (1200 ^{o}C), grain growth of the austenite was observed. Observed images are shown in Figure 5. 6. Grain boundary movements appear in circled areas. Detailed investigations into grain growth behaviors at high temperatures have already been conducted and reported in chapter 2.

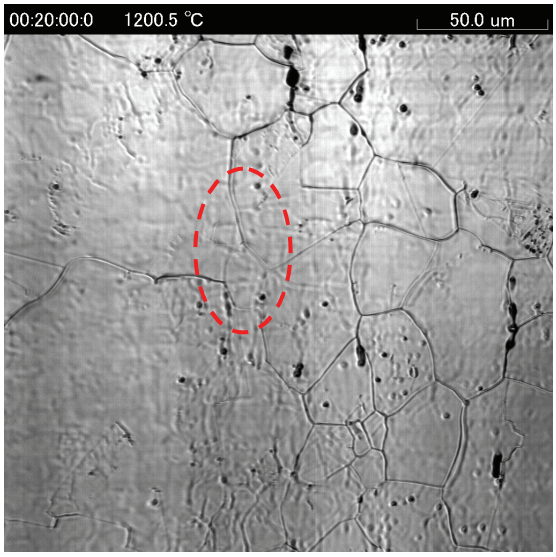

(a) Holding time at 1473 K: 0 s.

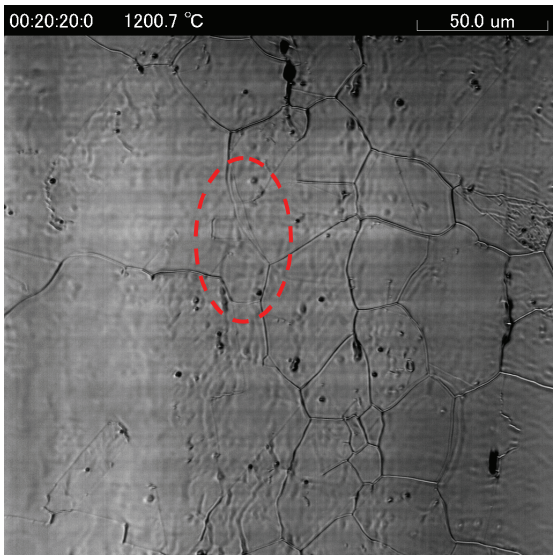

(b) Holding time at 1473 K: 20 s.

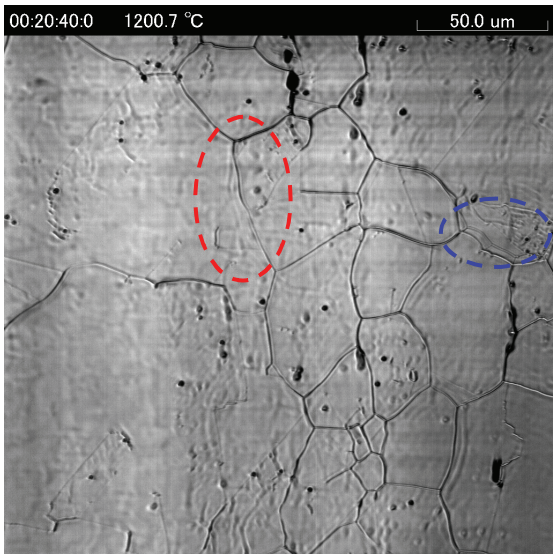

(c) Holding time at 1473 K: 40 s.

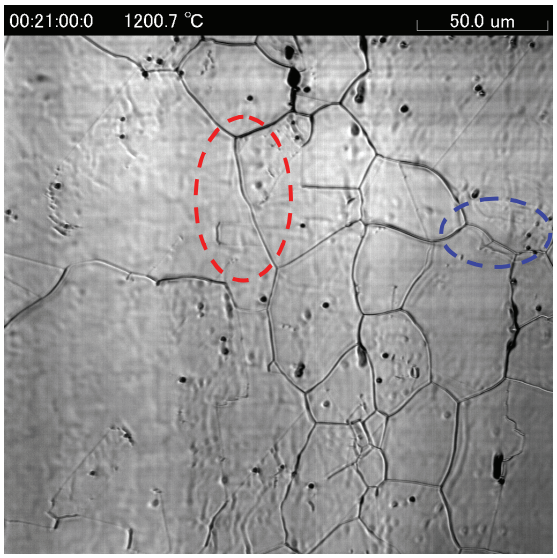

(d) Holding time at 1473 K: 60 s.

Figure 5. 6. Grain growth at 1473 K (1200 ºC).

5. 3. 3. Observed images while cooling

Observed images were captured every 200 K from an observation movie and shown in Figure 5. 7. From 1073 K (800 °C) to 873 K (600 °C), acicular ferrites appear.

In order to show images taken during phase transformation, from the austenite to the ferrite (allotriomorphic ferrite) and the pearlite, images at 948 K (675°C), 943 K (670°C), 938 K (665°C) and 933 K (660°C) were captured from the movie. Those are shown in Figure 5. 8. It is difficult to identify the movement of phase interface according to the captured images. However, advancing of phase interface can be clearly identified by observing the movie. The reason for the difficulties of observing microstructural changes would come from the thermal etching method. As mentioned in the chapter 2.2, unevenness such as grooves or facets on a specimen surface is observed by the laser microscope in the *in-situ* observation system. The interface between the austenite and the ferrite does not make grooves or facets. The interface is concavo-convex. While observing the movie, the movement of the concavo-convex interface can be found. On the other hand, by looking at the captured images from the movie, it is difficult to identify where the interface is.

Images at 923 K (650 °C), 921 K (648 °C), 919 K (646 °C) and 917 K (644 °C) were captured to show formation of acicular ferrites. Because acicular ferrites make up the facet interface, formation and growth of acicular ferrites are identified at circled area in Figure 5. 9.

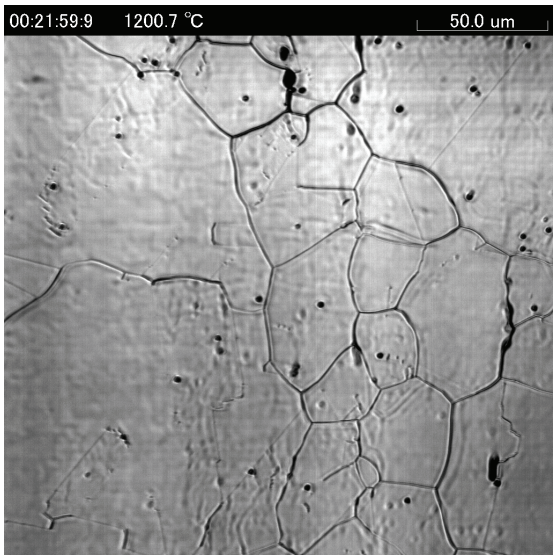

(a) 1473 K (1200 ºC)

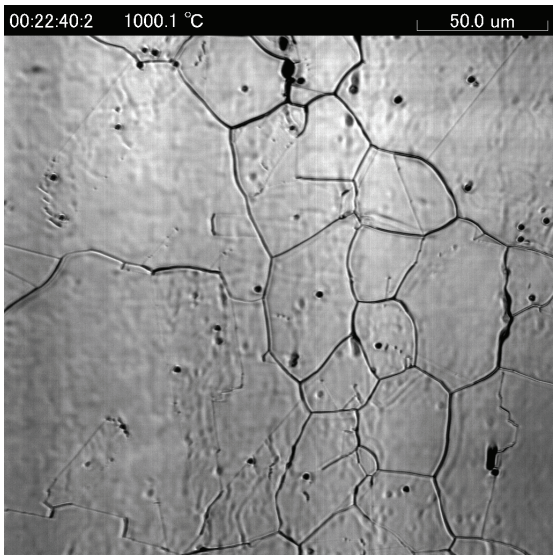

(b) 1273 K (1000 ºC)

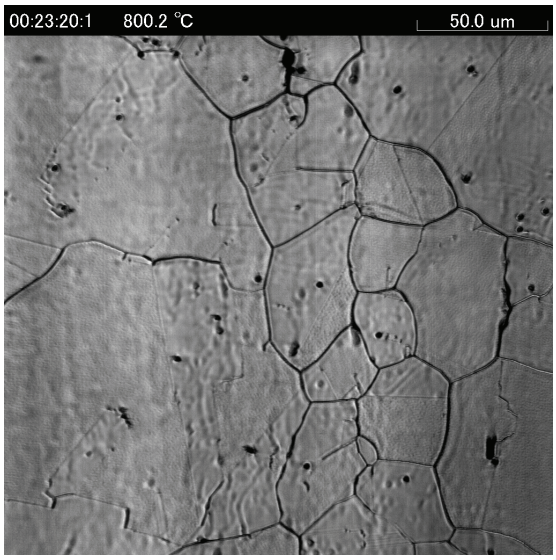

(a) 1073 K (800 ºC)

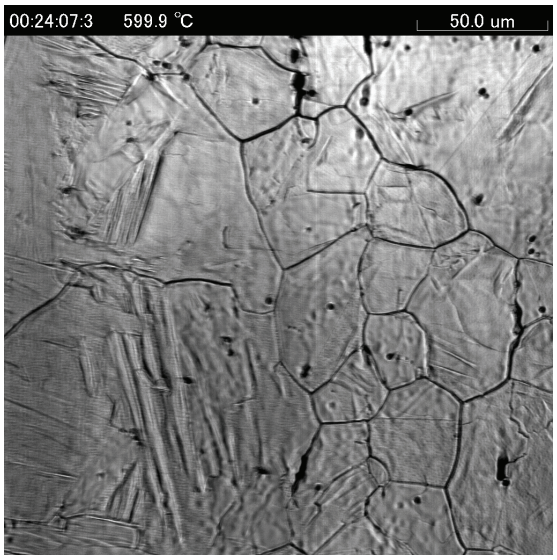

(b) 873 K (600 ºC)

Figure 5. 7. Observed images during cooling.

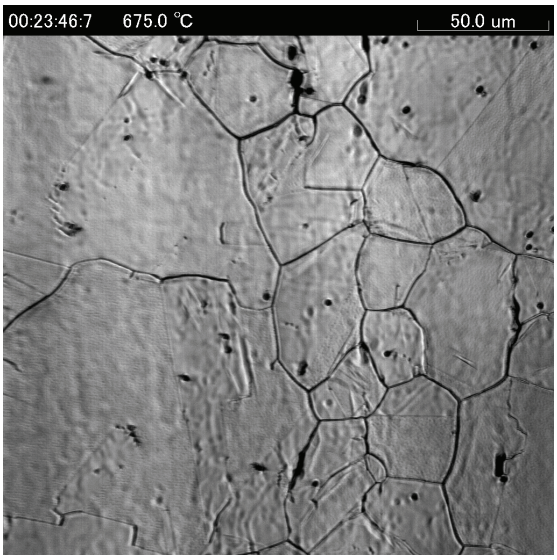

(a) 948 K (675 ºC)

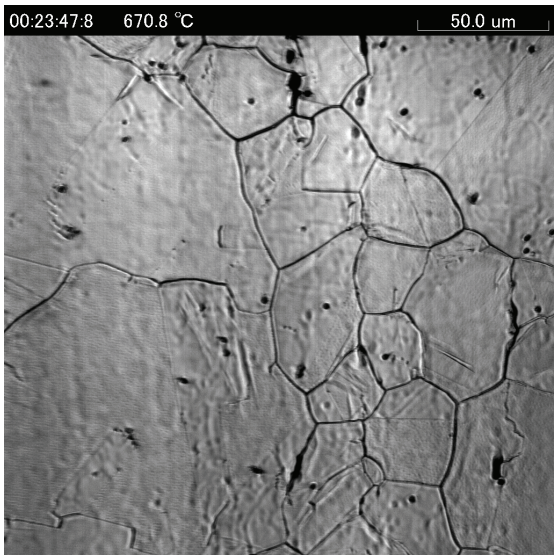

(b) 943 K (670 ºC)

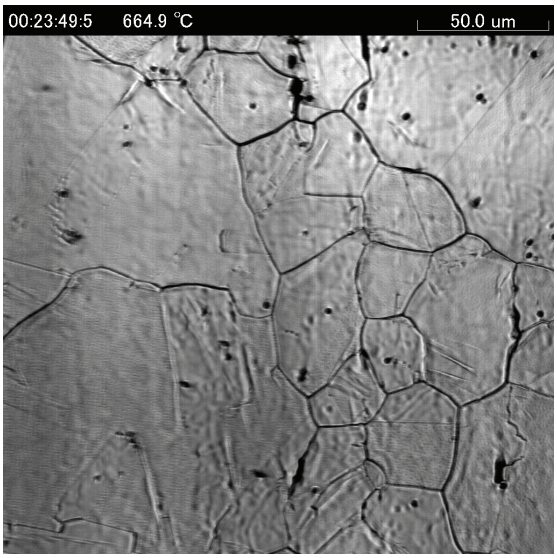

(a) 938 K (665 ºC)

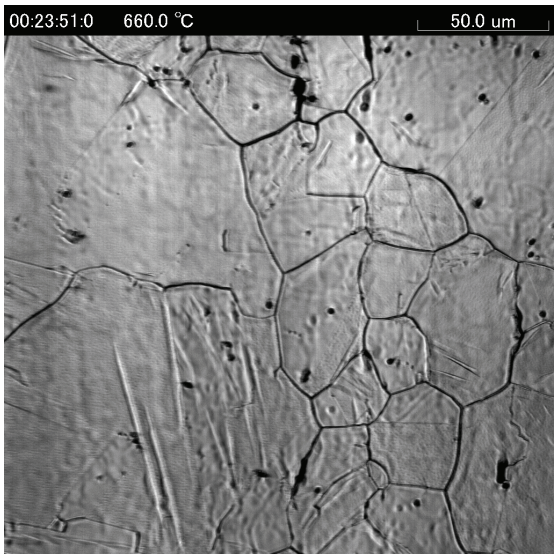

(b) 933 K (660 ºC)

Figure 5. 8. Movement of phase interface.

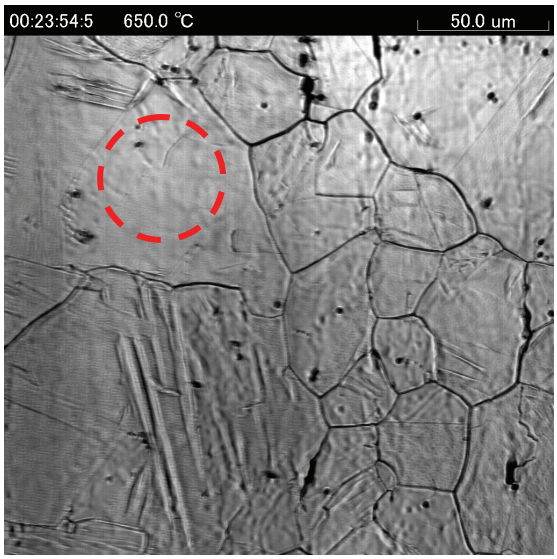

(a) 923 K (650 ºC)

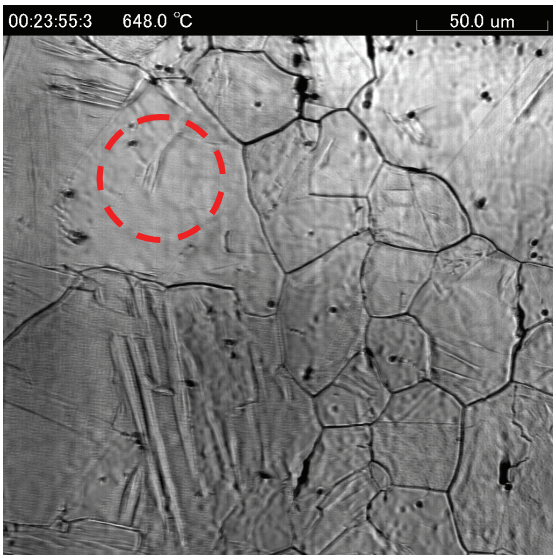

(b) 921 K (648 ºC)

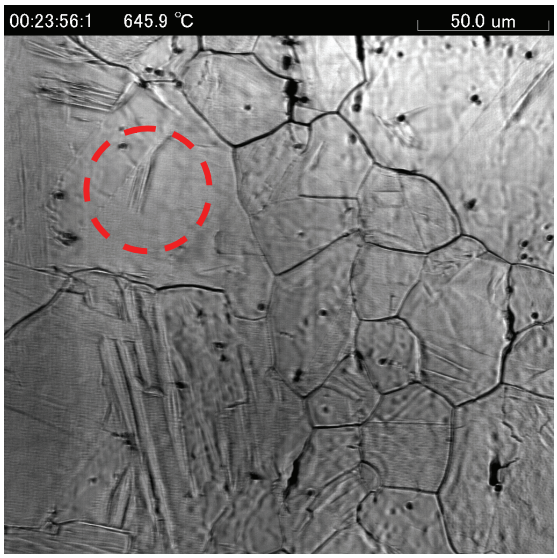

(a) 919 K (646 ºC)

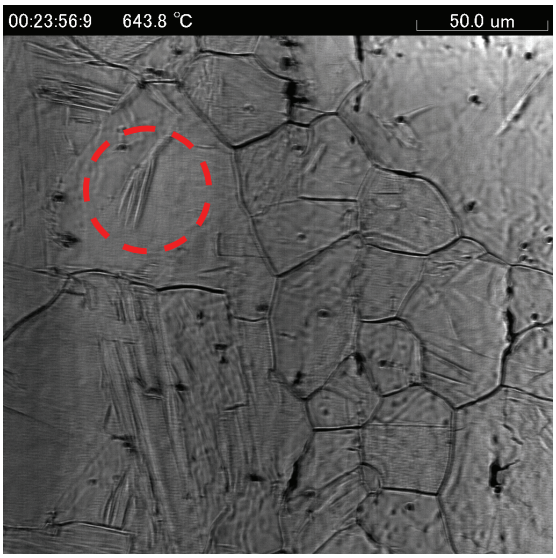

(b) 917 K (644 ºC)

Figure 5. 9. Formation and growth of acicular ferrites.

5. 3. 4. Comparison of images by a laser microscope to an optical microscope

For recognizing differences and characteristics of images taken by a laser microscope applied to the *in-situ* observation, two images were compared in Figure 5.10. An optical microscope can show color of microstructure. Therefore, as shown in Figure 5. 10 (a), the ferrite is colored with white and the pearlite is colored with black. On the other hand, a laser microscope scans the distance from the specimen's surface to a objective lens. Therefore, there is not any color information. In the case of images taken by a laser microscope, unevenness of the specimen's surface caused by the occurrence of new phases is observed. As shown in Figure 5. 10, it is possible to observe acicular ferrites using a laser microscope as well.

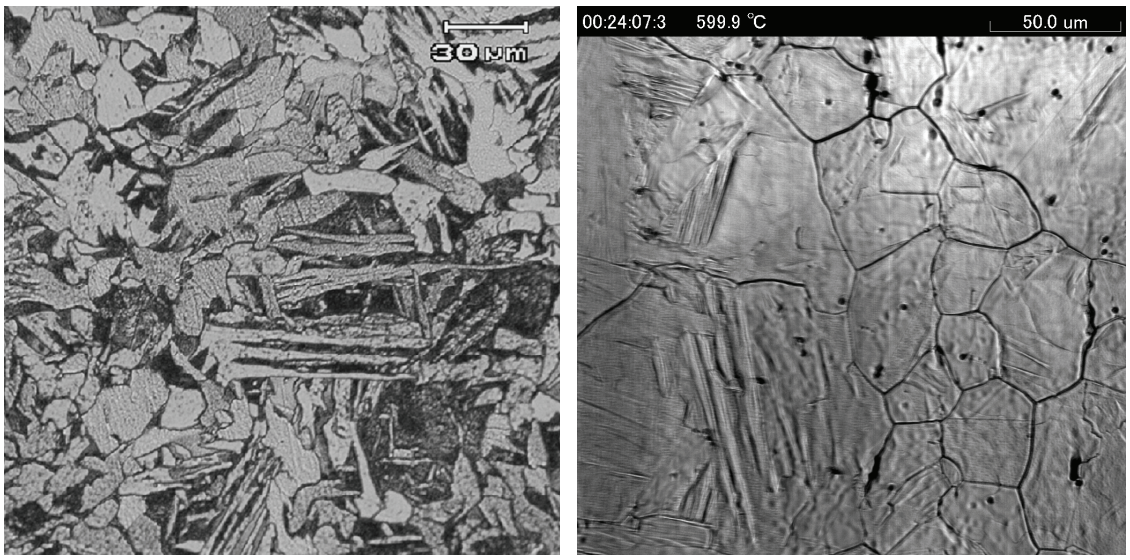

(a) By optical microscope (b) By laser microscope

Figure 5. 10. Comparison of observed images by optical and laser microscope.

5. 4. Conclusion

In this chapter, *in-situ* observations for inverse phase transformation and phase transformation were conducted. Because a laser microscope is not suitable to observe concavo-convex interfaces, it is not possible to observe the appearance of austenite during inverse phase transformation, and the movement of the interface between austenite and ferrite during phase transformation. On the other hand, the appearance of acicular ferrite which causes facet interface can be observed by the developed *in-situ* observation system.

According to the investigation in this chapter, it is expected that facet interfaces such as austenite / bainite and austenite / martensite interface will be observed by the developed *in-situ* observation system.

Chapter 6:

A calculation for grain growth rate of carbon steels by a solute drag model considering the segregation effect of each substitutional element

6. 1. Background

In order to produce high quality industrial parts made of metallic alloys, controlling the grain size by recrystallization and grain growth is an effective method. For control of the grain size, process conditions are typically determined using equation (1).

$$\left(\overline{D}\right)^n - \left(\overline{D}_0\right)^n = K \cdot t \qquad (1)$$

Here, $\overline{D}$ is the mean grain size, and $\overline{D}_0$ is the mean initial grain size. The parameters *K* and *n* are determined experimentally. Therefore, the grain size predicted by equation (1) is usually reliable for the corresponding experimental conditions. However, if the conditions used, such as temperature and chemical composition, are outside this range, the reliability of equation (1) becomes lower.

There is another method to predict the grain growth rate. This is not an experimental method as above, but rather is a method constructed theoretically. It is well known that when a grain boundary moves during grain growth, the solute contained within the grain boundary is dragged. This phenomenon is called solute drag. Various models incorporating mathematical descriptions for solute drag have been

proposed and subsequently improved by several authors. [6.1], [6.2], [6.3], [6.4] , [6.5] With these models, the concentration profiles across grain boundaries or phase interfaces can be calculated. The velocity of boundary movement during phase transformation and recrystallization were calculated by computing the balancing between dissipation energy and the driving force for solute drag. [6.6], [6.7], [6.8], [6.9]

In the solute drag model, the grain boundary property [6.4] is defined for expressing the difference in properties between the interior of the grain and the grain boundary. It is difficult to measure the grain boundary property for calculating the velocity of grain boundary movement. However, the difference in properties needs to be defined to simulate the solute drag effect and the interaction between the solute and grain boundary more realistically [6.10]. The interaction between the solute and the grain boundary is one of the causes of grain boundary segregation, especially in the case of microalloyed steels. Microalloyed Nb, V and Ti have a strong tendency to segregate at a grain boundary. These segregated elements retard boundary movement significantly in spite of low concentrations, even if the segregated elements do not form precipitates. For this reason, the segregation effect must be incorporated into the solute drag model. As far as I know, only a few studies have considered the segregation effect in the solute drag model based on experimental results. However, Nb was the only alloying element considered in these studies. [6.7], [6.9]

6. 2. Purpose of this study

The purpose of the present study is to develop a practical model for calculating

the grain growth rate including the influence of alloying elements and temperature. By coupling with thermodynamic calculations, the solute drag model can be applied to a wide range of alloying elements. Therefore, the solute drag model was chosen for this study. A model that incorporates the segregation effect and the procedure to determine the segregation energy for each substitutional element is first proposed, based on the solute drag model. Next, by using this model, the concentration profile across a grain boundary affected by the segregation effect of microalloying elements is calculated. Then, influence of solute drag into grain size evolution is discussed. Finally, in order to show the validity of the model, the temperature dependence of grain growth rate is calculated, and the results are compared with experimental results. This method would be the first development of the prediction method as a foundation of a new theoretically based prediction method for recrystallization.

6. 3. Modeling

6. 3. 1. Calculation of concentration profile across grain boundary

Odqvist el al. developed the model to calculate the deviation from local equilibrium at moving phase interfaces in multi-component systems. The method is based on finite interface mobility and solute drag theory [6.5]. According to the solute drag model [6.5], the concentration profile across a grain boundary during grain growth can be calculated by coupling equations (2) and (3).

$$\frac{v}{V_m}\left(u_k - u_k^{\alpha}\right) = J_k \qquad (2)$$

$$J_k = -\sum_{j=1}^{n-1} L''_{kj} \frac{\partial \phi_j}{\partial z} \quad (3)$$

Equations (2) and (3) represent fluxes of component *k* under steady state conditions of grain growth rate *v*, and the diffusion flux of component *k*, respectively. By solving the simultaneous equations (2) and (3), the concentration profile across a grain boundary at a grain growth rate *v* can be computed. α denotes the growing grain and V_m is the molar volume per substitutional atom. The *u*-fraction u_k is defined from the normal mole fraction x_k as

$$u_k = \frac{x_k}{\sum_l x_l} \quad (4)$$

where *l* in the denominator is substitutional atoms only. Therefore, if there are no interstitial elements, the *u*-fractions would be identical to the mole fractions. $\partial\phi_j$ is the gradient in diffusion potential which works as the driving force for diffusion. The diffusion potential is defined as $\phi_j = \mu_j - \mu_n$ where *j* is a substitutional solute and *n* is the solvent in a dilute solution. μ is chemical potential. The parameters L''_{kj} are related to the diffusion mobilities of different elements.

$$L''_{ki} = \sum_{j=1}^{n} \left(\delta_{ij} - u_i a_j\right)\left(\delta_{jk} - u_k a_j\right)\frac{u_j}{V_m} M_j \quad (5)$$

Here, δ_{ij} is the Kronecker delta with $\delta_{ij} = 0$ unless $i = j$. If the atom is a substitutional element, $a_j = 1$. On the other hand, if the atom is an interstitial element, $a = 0$. M_j is the intrinsic diffusional mobility of species j.

6. 3. 2. Balancing driving force and dissipation energy for grain growth

The balance between the driving force (ΔG^{tot}) and dissipation energy ($\Delta G^{sd} + \Delta G^{fric}$) yields equation (6).

$$\Delta G^{tot} = \Delta G^{sd} + \Delta G^{fric} \quad (6)$$

For calculating the grain growth rate, the driving force (ΔG^{tot}) is the excess energy that a polycrystal possesses over the energy of a single crystal. This excess energy is recognized as surface tension, explained by the Gibbs-Thomson effect. Therefore, the driving force is defined by equation (7). [6.11]

$$\Delta G^{tot} = \frac{2\sigma V_m}{\bar{r}} \quad (7)$$

Here, σ is the grain boundary energy and $\bar{r}$ is the mean radius of the grains. Total dissipation energy is energy resulting from the solute drag (ΔG^{sd}) in addition to dissipation of the Gibbs energy resulting from grain boundary friction (ΔG^{fric}). The two kinds of dissipation energy are defined by equations (8) and (9), respectively. [6.5]

$$\Delta G^{sd} = -\frac{V_m}{v}\sum_{i=1}^{n-1}\int_{-\infty}^{\infty} J_k\left(\frac{\partial \phi_k}{\partial z}\right)dz \quad (8)$$

$$\Delta G^{fric} = \frac{v}{M}V_m \quad (9)$$

Here, M is boundary mobility of a pure metal (not the intrinsic diffusional mobility, M_j). The grain growth rate at equilibrium between the driving force and total dissipation is the steady state velocity of grain growth, *v*.

In order to calculate grain size evolution, the following procedure should be applied. Dissipation energy of the solute drag is caused by grain boundary movement

with velocity, *v*. If grain boundary does not move, energy is not dissipated by the solute drag. The velocity, *v* is solved by equation (6) at first time increment. During grain growth with velocity, *v*, it is natural that grain size increases gradually. As a result of this, the driving force for grain growth decreases. Therefore, a grain size ($\bar{r}$) in equation (7) must be renewed, and then the velocity must be solved for the following time increment. This calculation flow corresponds to the suggestion [6.5] as "The net driving force is obtained after subtracting the capillarity effect if the interface is curved.".

6. 3. 3. Grain boundary modeling for the segregation effect

Some elements, especially microalloying elements, segregate at grain boundaries, and this significantly retards grain growth. Therefore, in order to calculate the grain growth rate, this segregation effect should be considered. According to a model by Hillert et al. [6.4] for an interface during phase transformation, an energy gap across the boundary is defined to make the model more realistic. In this study, a similar approach is applied to consider the segregation effect for the solute drag model. The segregation effect is introduced as segregation energy into the energy gap between the grain boundary and internal grain. The corresponding equations (3) and (8) are modified to (3)' and (8)'.

$$J_k = -\sum_{j=1}^{n-1} L''_{kj}\left(\frac{\partial \phi_j}{\partial z} + \frac{\partial \Delta G_k^{seg}}{\partial z}\right) \qquad (3)'$$

$$\Delta G^{sd} = -\frac{V_m}{v}\sum_{i=1}^{n-1}\int_{-\infty}^{\infty} J_k\left(\frac{\partial \phi_k}{\partial z} + \frac{\partial \Delta G_k^{seg}}{\partial z}\right)dz \qquad (8)'$$

ΔG_k^{seg} expresses the segregation energy of component *k*. It should be noted that ΔG_k^{seg} is non-dimentionalized by dividing RT as well as ϕ_k.

It is known that both (i) the difference in atomic diameter between a solvent and a substitutional element, and (ii) the solubility of a substitutional element strongly influence the segregation energy. [6.11], [6.12] In order to consider both factors in ΔG^{seg}, it is assumed to be expressed as equation (10).

$$\Delta G_k^{seg} / RT = \frac{\left(\Delta G_k^{solb} / RT\right)^A + \left(\Delta G_k^{dia} / RT\right)^B}{C} \qquad (10)$$

Here, ΔG^{solb} is the factor for the solubility and ΔG^{dia} is the factor for the difference in atomic diameter. *A, B* and *C* are parameters to be determined. Based on experimental results [6.11], ΔG^{solb} can be written as:

$$\Delta G_k^{solb} = \ln\left(1 / x_k^{solb}\right) \cdot RT \qquad (11)$$

By fitting experimental results [6.12], ΔG^{dia} derived from the difference in atomic diameter between the radius of the substitutional element (r^{subs}) and the radius of the solvent ($r^{solvent}$) is related by:

$$\Delta G_k^{dia} = 2000 \cdot \left(\frac{r_k^{subs} - r_k^{solvent}}{r_k^{solvent}} \right)^2 \qquad (12)$$

A grain boundary is divided into 3 zones. The central zone has an energy gap (ΔG^{seg}) from the interior of the grains. The properties of both side zones represent a

gradual change between the interior of the grain and the central zone. A schematic diagram of this grain boundary model is shown in Figure 6. 1.

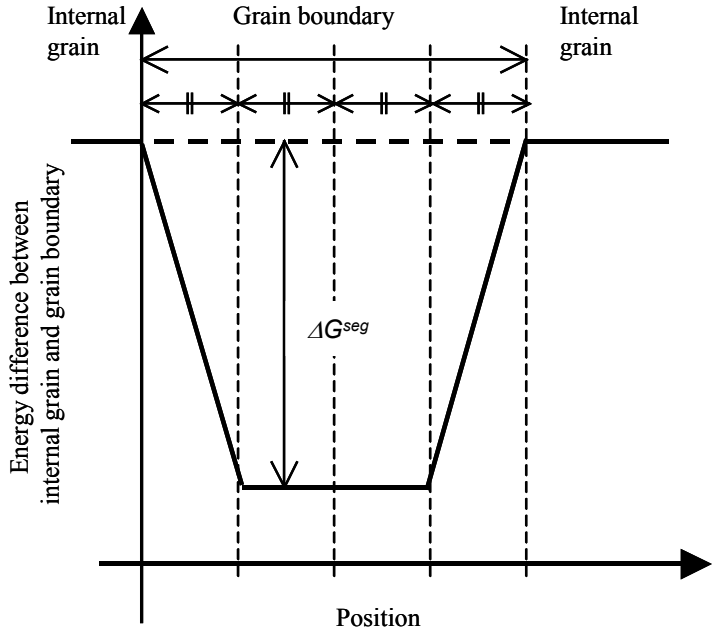

Figure 6. 1 The schematic diagram of a grain boundary model.

6. 3. 4. Estimation of contribution rate of solute drag for grain growth

In the proposed model, the velocity of grain boundary movement is calculated by the balance of the driving force and dissipation energy of the solute drag and boundary friction. In this section, contribution rate of the solute drag for grain growth in total dissipation energy is discussed.

In order to estimate the driving force, an average grain size ($\bar{r}$) is assumed as 50 μm. For the boundary mobility of a pure metal, estimation by Turnbull [6.13] is applied.

$$M = \frac{\delta D_{gb} V_m}{b^2 RT} \tag{13}$$

In this equation, δ is the grain boundary width, D_{gb} is the grain boundary self-diffusion coefficient and b is magnitude of the Burgers vector. According to equation (6), dissipation energy of the solute drag is estimated by $\Delta G^{sd} = \Delta G^{tot} - \Delta G^{fric}$. Contribution rate of the solute drag and boundary friction is shown in Figure 6. 2. In this figure, it is obvious that major contribution for grain growth is the solute drag in the range of velocity of grain growth. Therefore, it is important that estimation of dissipation energy of the solute drag be exact to calculate grain growth rate.

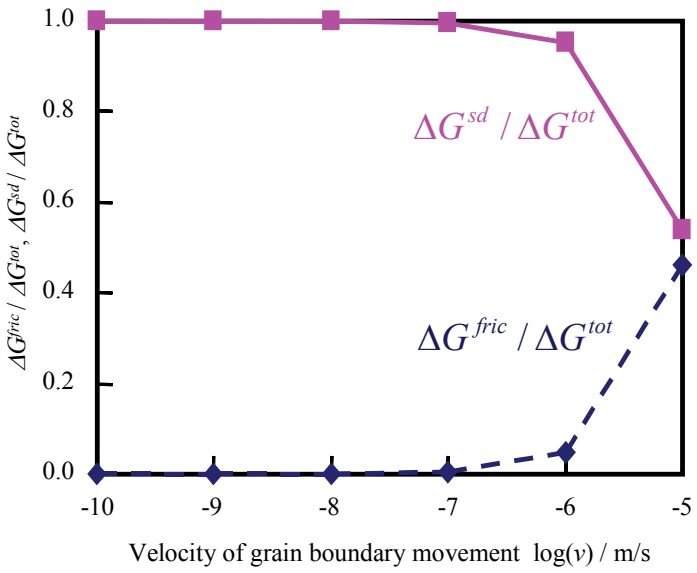

Figure 6. 2 The contribution rate of the solute drag and boundary friction for grain growth.

6. 4. Calculation results and discussion

6. 4. 1. Parameters determination

There are three unknown parameters (*A, B* and *C*) in equation (10). The process to determine those parameters is discussed here. If there are three simultaneous equations for three unknown parameters, the equations can be solved to determine the parameters. This is the basic concept for determining parameters *A, B* and *C*.

The grain growth rates at high temperatures in five steels were measured [6.14]. Grain growth rates measured in three steels without precipitations are applied for this study. The chemical compositions of the steels investigated are shown in Table 6. 1. The three materials represent a base steel without microalloying elements (steel 1), a V-alloyed steel (steel 2), and a (Nb and V)-alloyed steel (steel 3). Squared grain diameters measured were proportional to time, and the factors of proportionality were defined as rate constant. Substituting the rate constants in these three steels at 1473 K into equation (6), three simultaneous equations for parameters *A, B* and *C* can be prepared. By solving those equations numerically, the parameters *A, B* and *C* were determined. With this procedure for determining the parameters, the segregation energy is expressed by equation (14).

$$\Delta G_k^{seg} / RT = \frac{\left(\Delta G_k^{solb} / RT\right)^{0.24} + \left(\Delta G_k^{dia} / RT\right)^{1.30}}{9.0} \qquad (14)$$

The segregation energies of several elements determined by equation (14) at 1473 K are shown in Figure 6. 3. The energy derived from the difference in atomistic diameters between a solvent and a substitutional element, and the energy derived from the solubility of a substitutional element are also shown in Figure 6. 3. The values of 0.7 and 1.4 for the boundary energy were used by M. Hillert et al. [6.4] and M. Enomoto [6.6], respectively. (Concerning the value of 1.4, 8 kJ/mol was used originally in Ref. [6.6]. In Figure 6. 3, in order to non-dimensionalize the value for the Y-axis, the value of 1.4 is divided by RT.) The values determined by equation (14) are not very different from these values. Therefore, the values determined by equation (14) are presumably valid.

Table 6. 1 Chemical compositions of steels. [6.14]

Steel	C	Si	Mn	P	S	Al	Nb	V	N
1	0.06	0.05	1.58	0.0012	0.0012	0.027	-	-	0.0056
2	0.06	0.05	1.24	0.0013	0.0012	0.029	-	0.12	0.0055
3	0.06	0.05	1.26	0.0012	0.0012	0.028	0.046	0.06	0.0048

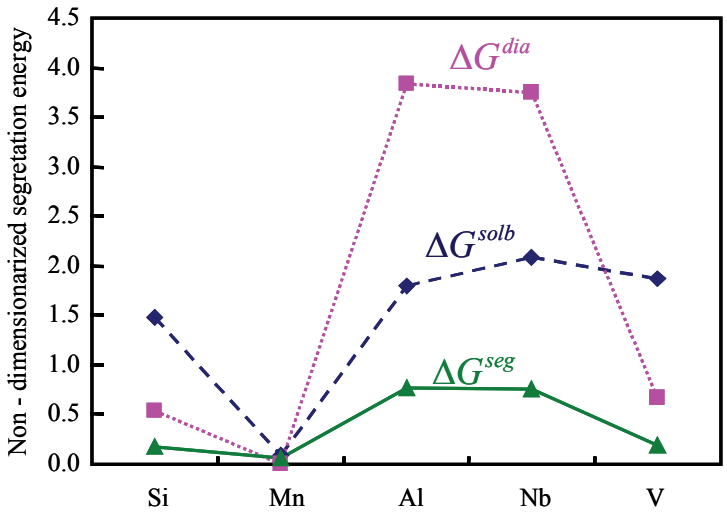

Figure 6. 3 Determined segregation energy of elements.

6. 4. 2. Calculation conditions

The calculation procedure was coded using the Fortran programming language. The concentration profile across a grain boundary was solved with the forward difference method. It is known that the grain boundary energy (σ) changes depending on the kinds of alloying elements and their quantity. However, the grain boundary energy is defined as 0.2 J/m^2 for all steels since all influence of alloying elements are considered in equation (14) of this study. The width of the grain boundary was defined as 1×10^{-9} m, and calculation length was defined as 3 times the width of the grain boundary. The total number of grid points for a calculation was 601. The diffusion flux (ϕ) in each grid was calculated using Thermo-Calc ver.S [6.15] software along with the thermodynamic database TCFE6. Thermo-Calc is based on the minimization of the total Gibbs energy of the system and on the CALPHAD approach. [6.16], [6.17], [6.18] The Fortran program was compiled with the Thermodynamic Calculation Interface to connect to Thermo-Calc.

6. 4. 3. Changing of concentration profile and grain size evolution

The concentration profile across a grain boundary was calculated for steel 3, which contains Nb and V, with and without consideration of segregation energy. The following calculation conditions were used: grain growth rate of 1.0×10^{-8} m/s and temperature of 1473 K. The segregation energy for each element was determined by equation (14) and applied for the calculation considering the segregation energy. In the case of the calculation without consideration of the segregation energy, the value

determined for Mn by equation (14) was defined as the segregation energy for all elements.

The calculated concentration profiles are shown in Figure 6. 4. In Figure 6. 4, y-axis shows segregation of each element. u and u_0 mean that the u-fraction within grain boundary and average concentration in bulk, respectively. x-axis is normalized by the width of the grain boundary. The concentration profile calculated without consideration of the segregation energy shows a tendency for the element, which has higher initial concentration, to have higher concentration at a grain boundary as well. On the other hand, the concentration of Nb increased significantly with consideration of the segregation energy. Figure 6. 5 shows comparison of maximum segregation within grain boundary between the calculation with and without consideration of the segregation effect. It is recognizable that high magnitude of segregation by the calculation with consideration of the segregation effect is a cause of retardation of grain growth.

In the following, grain size evolution is calculated. Calculated grain diameter and driving force of steel 2 at 1473 K are shown in Figure 6. 6. In Figure 6. 7, the comparison of grain size evolution between experiment and calculations is shown. Three types of calculations are conducted: the proposed model, the model without considering the segregation effect of each substitutional element and the model considering only boundary friction. The experiment and the only calculation by the proposed model show reasonable correspondence. It means that it is necessary when calculating grain growth rate to consider the solute drag and the segregation energy of

each substitutional element.

Next, the reason why the relationship between squared grain diameter and time is proportional is discussed. Figure 6. 8 shows the relationship between velocity of grain boundary moving and dissipation energy of the solute drag. In the range of velocity for grain growth, dissipation energy of the solute drag is proportional to velocity of grain boundary. Therefore, dissipation energy can be represented by $\Delta G^{sd} = C \cdot v = C \cdot \frac{d\bar{r}}{dt}$. Because of low contribution rate of boundary friction discussed in the section 6.2.2, the relationship between the driving force and dissipation energy can be written as $\frac{2\sigma V_m}{\bar{r}} = C \cdot \frac{d\bar{r}}{dt}$. This equation can be simplified as $t = C' \cdot \bar{r}^2$. As a result of that, squared grain diameter is proportional to time.

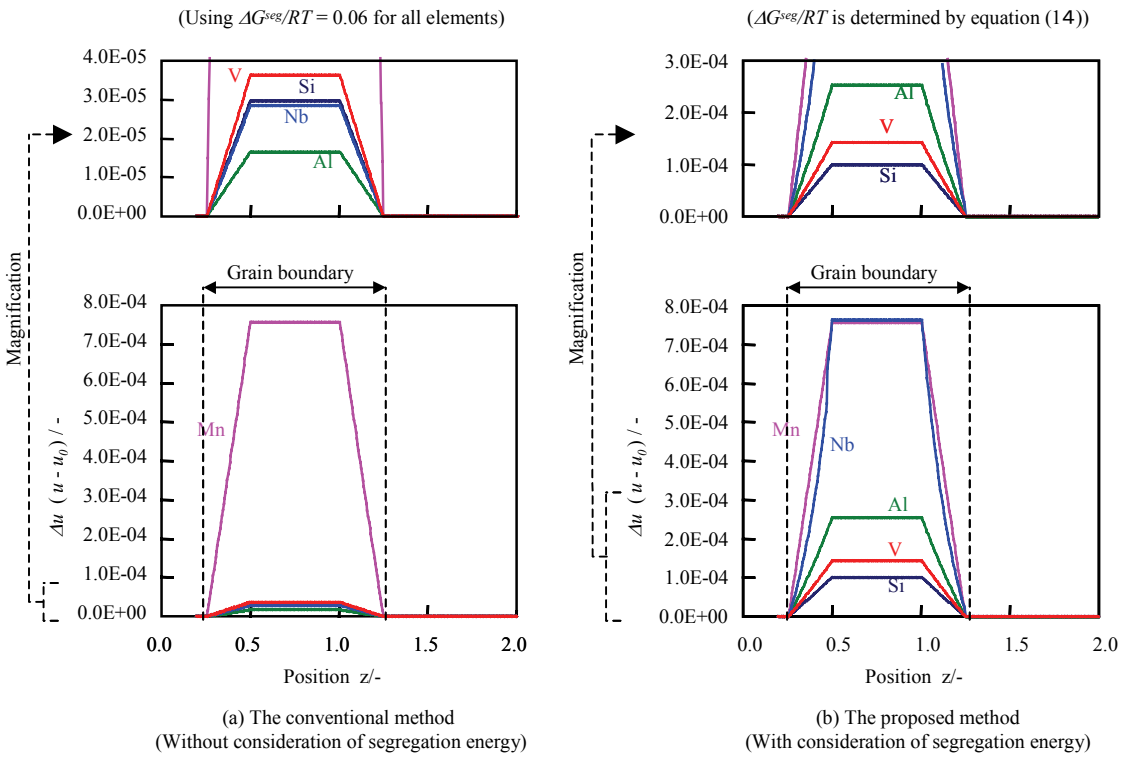

Figure 6. 4 Calculated concentration profile across a grain boundary of steel 3

($v = 1.0\times10^{-8}$ m/s)

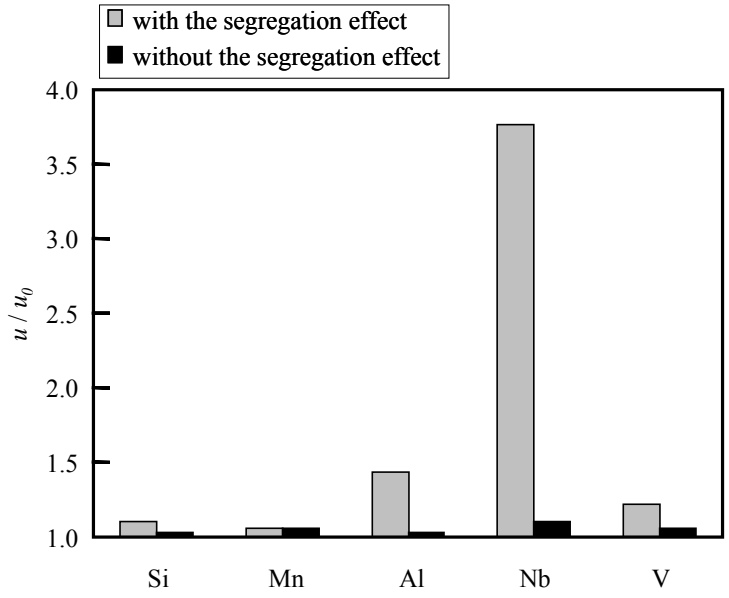

Figure 6. 5 Comparison of maximum segregation within grain boundary of steel 3 between the calculation with and without consideration of the segregation effect.

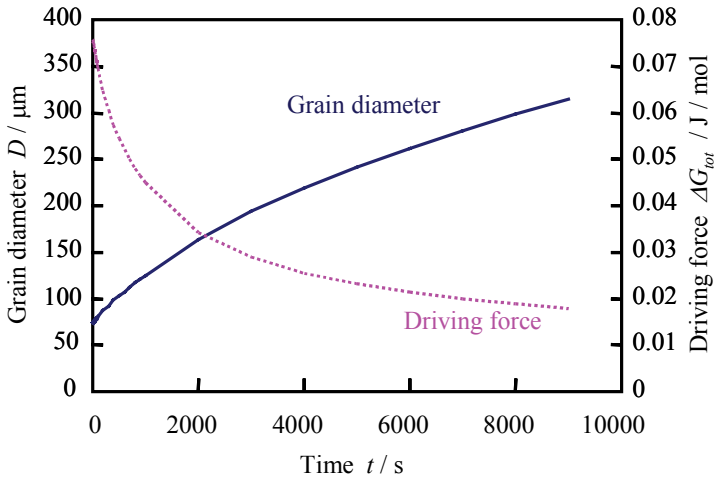

Figure 6. 6 The change of grain diameter and driving force of steel 2.

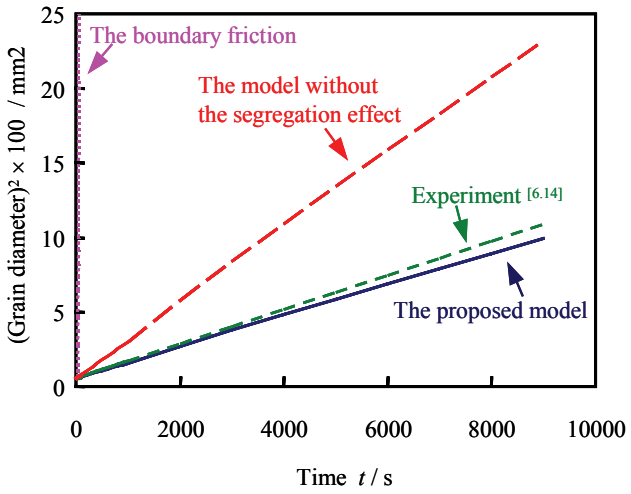

Figure 6. 7 Comparison of grain growth of steel 2 between experiment and models.

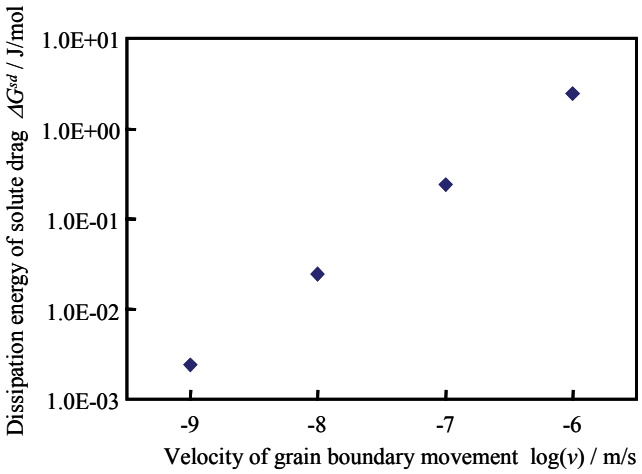

Figure 6. 8 Dissipation energy of the solute drag.

6. 4. 4. Calculation of temperature dependence of grain growth rate

The proposed model offers the possibility to simulate temperature dependence of the grain growth rate. This is because the diffusion potential (ϕ), the solubility limit in ΔG^{solb} and the intrinsic diffusional mobilities of species (M_j) are included in the proposed model. All of these factors have a temperature dependence. For the three materials in Table 6.1, the grain growth rates at 1423, 1473 and 1523 K are calculated by the proposed model. According to the experimental results [6.14], the initial grain size ($\bar{r}$) for the driving force is determined at each temperature. Equation (6) is a non-linear equation, therefore the grain growth rate is solved by iterations. As mentioned above, squared grain diameter is proportional to time. Therefore that relationship is described as

$$D^2 = K \cdot t \qquad (15)$$

A comparison of the rate constant (K) is shown in Figure 6. 9. It is natural that the calculated results at 1473 K show reasonable correspondence, since the parameters in equation (14) were determined to fit the calculation results at 1473 K to the experimental results at 1473 K. On the other hand, the same parameters in equation (14) are given for the calculations at 1423 and 1523 K. The calculation results at 1423 and 1523 K simulate the influence of the microalloying elements and temperature well. These correspondences show the validity of the proposed model, which incorporates the segregation effect into the solute drag model, and its potential to predict the influence of alloying elements and temperature dependence.

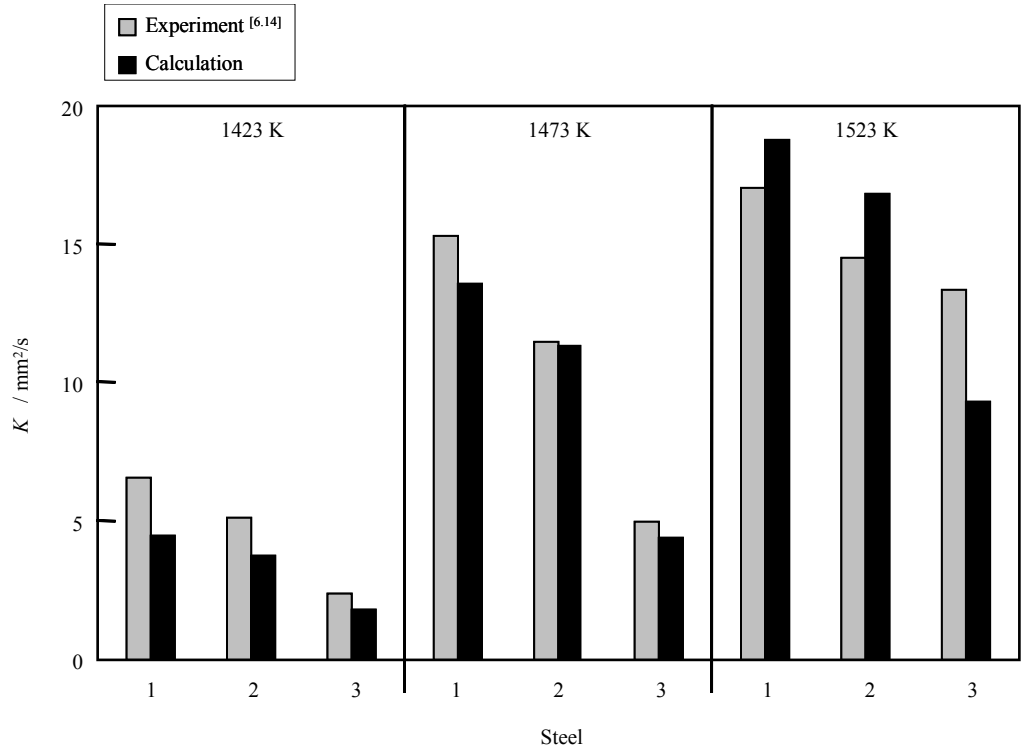

Figure 6. 9 Comparison of grain boundary velocities between experiments and calculations.

6. 5. Conclusion

A practical model to calculate grain growth rate has been developed. This model is based on the solute drag model incorporating the segregation effect. Using this model, the concentration profiles across grain boundaries and grain size evolution were calculated. The calculated results to simulate the influence of microalloying elements and temperature for grain growth show reasonable agreement with experimental results.

Reference

[6.1] K. Lucke and K. Detert: Acta Met., 5 (1957), p. 628-637.

[6.2] J. W. Cahn: Acta Met., 10 (1962), p. 789-798.

[6.3] K. Lucke and H. Stuwe: Recovery and Recrystallisation, (1963), p. 131.

[6.4] M. Hillert and B. Sundman: Acta Met., 24 (1976), p. 731-743.

[6.5] J. Odqvist, B. Sundman, J Agren: Acta Mat., 51 (2003), p. 1035-1043.

[6.6] M. Enomoto: ISIJ Int., 47 (1999), p. 3533-3540.

[6.7] M. Suehiro, Z. K. Liu, J Agren: Acta Mat., 44 (1996), p. 4241-4251.

[6.8] M. Suehiro, Z. K. Liu, J. Agren: Met. Mat. Trans., 29A (1998), p. 1029-1034.

[6.9] M. Suehiro: ISIJ Int., 38 (1998), p. 547-552.

[6.10] M. Schalin, B. Sundman: TRITA-MAC-623(1999)

[6.11] Mikurososhiki-no-Netsurikigaku, The Japan Institute of Metals, (2005), p. 135-145 (in Japanese)

[6.12] T. Nishizawa: Materia Japan, 40 (2001), p. 437-441.

[6.13] D. Turnbull: Trans. AIME, 191 (1951), p. 661-665.

[6.14] H. Kobayashi: Tetsu-to-Hagane, 63 (1977), p. 73-79 (in Japanese).

[6.15] M. Hillert: in Computer Modeling of Phase Diagrams, L.H. Bennett, ed., TMS-AIME, Warrendale, PA, 1986, pp. 1-17.

[6.16] J. Ågren: Current Opinion in Solid State & Materials Science, 1996, vol. 1, pp. 355-60.

[6.17] B. Sundman: Scand. J. Metall., 1991, vol. 20, pp. 79-85.

[6.18] B. Jansson, B. Jönsson, Bo. Sundman, and J. Ågren: Thermochimica Acta, 1993, vol. 214, pp. 93-96.

Chapter 7:

Summary

In order to develop a theoretical model to predict grain size change during recrystallization, detailed investigations must first be conducted. By the conventional method, which requires a specimen to cool down to room temperature, microstructural changes during recrystallization cannot be observed. Therefore, in this study, development of the method suitable for observations of microstructural changes has been conducted.

In chapter 2, the *in-situ* observation method has been developed. That observation method enables us to observe microstructural changes at high temperatures. By using that observation method, grain growth at high temperatures (1273 - 1523 K) was observed, and grain size changes during grain growth were analyzed in detail. In chapter 3, *in-situ* observations during application of small strains were conducted to observe strain induced boundary motion (SIBM). Characteristics of SIBM, such as initiating strain for SIBM and velocity of SIBM were measured by the results of the *in-situ* observation. In chapter 4, dynamic recrystallization was observed by the *in-situ* observation method. These results were the first observation of microstructural changes during hot deformation at 1473 K, which was until now, considered very difficult to observe. In chapter 5, the *in-situ* observation was applied to observation for phase transformation during heating and cooling. Through these studies, it is confirmed that

the developed *in-situ* observation method can be applied to observations for a wide range of microstructural changes during hot deformation, heating and cooling.

In the following, as a fundamental of the theoretical model to predict grain size change during recrystallization, a theoretically based model for predicting grain growth was developed. The developed model is based on the solute drag theory and coupled with thermodynamic calculations. Therefore, the model can be applied to evaluate the influence of major alloying element for forging steels into grain growth. The developed model for grain growth has the possibility to apply recrystallization by renewing the driving force and considering nucleation of recrystallized grain.

The theoretically based prediction method for grain size change during recrystallization will be developed by combining detailed observation results for recystallization using the *in-situ* observation method with the developed prediction model. This work should be a future challenge.

List of publications:

[1] In-Situ Observation of Grain Growth of Steel at High Temperature

Yasuhiro Yogo, Kouji Tanaka, Koukichi Nakanishi, Materials Transactions, Vol. 50, pp.280-285 (2009)

[2] In Situ Observation Method for Microstructural Changes of Steel During Hot Deformation

Yasuhiro Yogo, Hirohisa Takeuchi, Kouji Tanaka, Noritoshi Iwata, Koukichi Nakanishi, Takashi Ishikawa: Microscopy Research and Technique, Vol. 72, pp.899-901 (2009)

[3] Strain-induced boundary migration of carbon steel at high temperatures

Yasuhiro Yogo, Hirohisa Takeuchi, Takashi Ishikawa, Noritoshi Iwata, Koukichi Nakanishi: Scripta Materialia, Vol. 61, pp.1001-1003 (2009)

[4] In-situ Observation of Grain Growth and Recrystallization of Steel at High Temperature

Yasuhiro Yogo, Kouji Tanaka, Koukichi Nakanishi: Materials Science Forum, Vols. 638-642, pp. 1077-1082 (2010)

[5] A calculation for grain growth rate of carbon steels by a solute drag model considering the segregation effect of each substitutional element

Yasuhiro Yogo, Kouji Tanaka, Hideaki Ikehata, Noritoshi Iwata, Koukichi Nakanishi, Takashi Ishikawa: Materials Science and Technology, Accepted on 20/10/2010

Acknowledgement:

I wish to thank TOYOTA CENTRAL R&D LABS., INC. for providing me to an opportunity to carry out this research and for their financial support.

I would like to express my gratitude to Professor T. Ishikawa at Nagoya Univ. as the supervisor of this research, for stimulating discussions, and students of his laboratory for their friendship.

I gratefully acknowledge Dr. K. Nakanishi, Dr. N. Iwata and Dr. K. Tanaka at TOYOTA CENTRAL R&D LABS., INC. for their continuous encouragement, kind advice and important discussions. I am indebted to Mr. H. Takeuchi and Mr. E. Ohta for their kind help in conducting experiment. Many thanks also to my other colleagues.

I wish to express my special thanks to my wife for her dedicated support in accomplishing this research, I am also grateful to my lovely daughter. Finally, I deeply thank my parents for their cordial encouragement and love throughout my life.